Geochemical constraints on mantle sources and basalt petrogenesis in the Strait of Sicily Rift Zone (Italy).

To be submitted to *Lithos*

John Charles White[1,*], David A. Neave[2], Silvio G. Rotolo[3, 4], and Don F. Parker[5, †].

[1]Department of Geosciences
Eastern Kentucky University
521 Lancaster Ave., Science 2234
Richmond, KY 40475 USA

[2]School of Earth and Environmental Sciences
The University of Manchester
Oxford Road, Manchester
M13 9PL, UNITED KINGDOM

[3]Dipartimento di Scienze della Terra e del Mare (DiSTeM)
Università di Palermo
Via Archirafi 36
90123 Palermo ITALY

[4]Instituto Nazionale di Geofisica e Vulcanologia (INGV)
Sezione di Palermo
Via Ugo La Malfa 153
90146 Palermo ITALY

[5]Department of Geosciences
Baylor University
Waco, TX 76798 USA

*Corresponding author: john.white@eku.edu (e-mail), +1 859-622-1276 (phone), +1 859-622-3357 (fax).

† Present address: School of Math and Science, Wayland Baptist University, 1900 West 7th Street, Plainview, TX 79072 USA

Abstract

Basaltic magmatism from the late Miocene to historic time (most recently 1891 CE) in the Strait of Sicily has created two islands (Pantelleria and Linosa) and several seamounts. These volcanoes are dominated by transitional (ol+hy-normative) to alkaline (ne-normative) basaltic lavas and scoriae; consanguineous peralkaline felsic rocks occur only on Pantelleria. Although most likely erupted through continental crust, basalts demonstrate no evidence of crustal contamination and are geochemically similar to oceanic island basalts (OIB). Despite these broad similarities, there are considerable compositional differences both between and within the two islands that are due to short-length scale mantle heterogeneity beneath the region as well as variability in partial melting and magma storage conditions. The results of geochemical modelling suggest that lithospheric thickness beneath both islands is ~60 km, consistent with published geophysical models, with a mantle potential temperature between 1400-1450°C, similar to other documented continental "passive rifts," such as the Basin and Range province (USA). Linosa basalts were formed from ~2-3% partial melting of a source region dominated by depleted MORB mantle (DMM) well-mixed with a small fraction of recycled MORB lithosphere (as eclogite or garnet pyroxenite) originating in the garnet-spinel transition zone. Trace element evidence suggests Pantelleria basalts were formed by ~3-4% partial melting of a source also consisting of DMM, but with a much higher proportion of recycled MORB lithosphere and an additional LILE-enriched component, with melting of lithologically enriched material beginning as deep as ~116 km. On both islands, storage of basaltic magmas occurred primarily at two levels: 0.5 GPa, corresponding to the Moho (17-25 km); and 0.2-0.1 GPa, corresponding to the top of the crystalline basement (8-4 km). Magmas stored in the higher-level chamber were more effectively homogenized and thus have a narrower compositional range. Despite the geophysical

similarities between the two islands in terms of lithospheric thickness and crustal thinning, melt productivity has been historically greater at Pantelleria, producing a much larger island, which may ultimately be entirely due to the local occurrence of much more fusible mantle.

Keywords: Strait of Sicily Rift Zone, Continental-OIB, Alkali Basalt, Mantle Melting, Mantle Heterogeneity

1. Introduction

The Mediterranean Sea between the island of Sicily and the Tunisian coast is the setting for magmatism with an OIB-like affinity that has produced two islands (Pantelleria and Linosa) and several seamounts which occur subparallel to the faulted margins of two of the three northwest-southeast trending grabens that comprise the Strait of Sicily Rift Zone (SSRZ) (Figure 1; Catalano et al., 2009). Transitional (hy+ol-normative) to alkali (ne-normative) basaltic lavas and tuffs occur throughout the SSRZ, with evolved rocks (peralkaline trachyte and rhyolite [pantellerite]) occurring only at Pantelleria, where they form in a bimodal association typical of intraplate magmatic settings (Mahood and Hildreth, 1986; Civetta et al., 1998; Bindi et al., 2002; Rotolo et al., 2006; Di Bella et al., 2008; White et al., 2009; Neave et al., 2012; Avanzinelli et al., 2014).

It was noted early that the major- and trace-element variation at Pantelleria could not be attributed to polybaric fractional crystallization of a single parental magma and required instead multiple parental magmas related by varying degrees of partial melting from a garnet peridotite source (Mahood and Baker, 1986). Subsequent studies revealed that the mantle source is nearly isotopically homogenous: basalts throughout the rift zone have nearly identical Sr-isotopes

Commentato [DN1]: I understand what you mean here, but I think mentioning OIB quite so early could be a bit of a red herring. Maybe a different tone would read better? Perhaps "the setting for magmatism with a OIB-like affinity" or something like that? I'm not sure we have the answer to why this is the case, but you make a very compelling case here for the conditions under which the SSRZ magmas have been generated.

(Linosa: 0.7031 ± 0.0001; Pantelleria: 0.7032 ± 0.0001; Seamounts: 0.7035 ± 0.0005) and very similar Nd-isotopes (Linosa: 0.51291-0.51297 [ε_{Nd} = 5.9 ± 0.5]; Pantelleria: 0.51287-0.51299 [ε_{Nd} = 6.2 ± 0.4]; Seamounts: 0.51299-0.51312 [ε_{Nd} = 7.7 ± 0.5]) (Esperança and Crisci, 1995; Civetta et al., 1998; Rotolo et al., 2006; Di Bella et al., 2008; Avanzinelli et al., 2014). Lead isotope ratios both between and within the volcanic centers are more variable, becoming more radiogenic from the older (1070 to 530 ka) Linosa suite to the paleo-Pantelleria suite (120-80 ka), with the younger (29-10 ka) neo-Pantelleria suite and Seamounts showing intermediate values (Rotolo et al., 2006; Avanzinelli et al., 2014). These isotopic data place the Pantelleria and Linosa basalts on the mantle array in the compositional space assigned to "Prevalent Mantle" (PREMA) between depleted MORB mantle (DMM) and an enriched component frequently identified as HIMU (High-μ, $\mu = {}^{238}U/{}^{204}Pb$) (Zindler and Hart, 1986; Stracke, 2012). Helium isotopes recorded at both Pantelleria and Linosa are similar ($^{3}He/^{4}He$ = 7.3-7.6 R/R_a; Parello et al., 2000; Fouré et al., 2012), lower than global MORB (8.3 R/R_a) and also similar to HIMU islands (6.8 ± 0.9 R/R_a; Hanyu and Kaneoka, 1997). Based on these results, mantle sources for basaltic magmatism in the SSRZ have been variably interpreted as: (1) lithospheric mantle chemically modified by the addition of recycled MORB material (Esperança and Crisci, 1995); (2) depleted MORB mantle enriched by a fossil "plume" of deep mantle material (Civetta et al., 1998; Rotolo et al., 2006); (3) a mixture of asthenospheric and metasomatized lithospheric mantle (Di Bella et al., 2008); or (4) asthenosphere enriched with an eclogitic component representing recycled MORB material (Avanzinelli et al., 2014). In their study, Avanzinelli et al. included the results of U-series disequilibrium systematics for the neo-Pantelleria lavas and concluded that the sources are strictly asthenospheric, with no need for interaction with lithospheric mantle or continental crust nor any need for a metasomatic component (viz., no role for amphibole). Further, they suggested a positive correlation exists between radiogenic Pb and a greater amount of recycled material.

Differences in basalt major- and trace-element chemistry have also been documented both between and within the islands and seamounts. At Pantelleria, Civetta et al. (1998) divided the basalts into "High Ti-P" and "Low Ti-P" types, with the former also characterized by higher concentrations of incompatible trace elements and higher LREE/HREE than the latter, which they attributed to different degrees of partial melting from a locally heterogeneous asthenospheric mantle. Similar differences were described on Linosa, where Di Bella et al. (2008) recognized a "Trend-A" and "Trend-B", with the former having higher K_2O, P_2O_5, incompatible trace elements (e.g., Rb, Th), and LREE/HREE at a given value of MgO. Although Di Bella et al. attributed the differences between the volcanic centers of the SSRZ to varying degrees of partial melting from heterogeneous mantle sources, they modelled the Linosa trends as differentiates from a common primary magma. In our paper we present the results of major-element, trace-element, and thermodynamic geochemical models for Pantelleria, Linosa, and the seamounts that attempt to: (1) constrain the magma storage conditions in the crust and describe its effect on basalt geochemistry; (2) determine the conditions of partial melting in the asthenosphere beneath the SSRZ; (3) discriminate between the effects of lithospheric thickness, source lithology, and magma storage on the geochemistry of these basalts; and (4) attempt to characterize the nature of the enriched mantle component(s) in the SSRZ asthenosphere.

2. Geologic Setting

The Strait of Sicily Rift Zone (SSRZ) is a northwest-southeast trending transtensional rift system situated on the Hyblean-Pelagian Block, the northern promontory of the African plate that represents the foreland domain of the Sicilian Apenninic-Maghrebian orogen (Catalano et al., 2009, and references therein). The SSRZ consists of three basins: the Pantelleria Trough, the Linosa Trough, and the Malta Trough. Water depth is <500 m beneath most of the Pelagian Block, increasing to ~1350 m in the Pantelleria Trough, ~1580 m in the Linosa Trough, and ~1720 m in the Malta Trough (Calanchi et al., 1989). Volcanoes are present in or adjacent to all except the Malta Trough, and include two islands (Pantelleria and Linosa) and several seamounts. The thickness of the crust throughout most of the Pelagian Block is 25-35 km, thinning to 16-18 km beneath the troughs, 20-21 km beneath the island of Pantelleria, and 24-25 km beneath the island of Linosa (Civile et al., 2008; Catalano et al., 2009). The depth to the lithosphere-asthenosphere boundary has been inferred from regional geophysical studies. The Pelagian Block is characterized by high heat flow (>80 mW/m^2) with values that increase to >130 mW/m^2 in the Pantelleria and Linosa troughs (Della Vedova et al., 1995) and up to 200-460 mW/m^2 within the Cinque Denti caldera (Bellani et al., 1995). Combined with positive Bouguer anomalies (65-103 mgal; Berrino and Capuano, 1995), several workers have suggested asthenospheric upwelling up to ~60 km (Della Vedova et al., 1995; Argnani and Torelli, 2001; Civille et al., 2008).

Extension of the SSRZ began about 9-10 Ma, with minor volcanism occurring during the late Miocene (Tortonian-Messinian) and the vast majority of volcanism occurring during the Plio-Pleistocene. (Calanchi et al., 1989; Rotolo et al., 2006; Coltelli et al., 2016; Lodolo et al., 2019). Volcanic seamounts are primarily located in one of three areas within the SSRZ (Aissi et al., 2015): (1) the Graham and Terrible volcanic province (Anfirite, Tetide, Galatea, Graham Bank, Cimotoe, Pinne, and Nameless Bank volcanoes) which lies 50-75 km offshore and runs parallel to the coast of Sicily for ~100 km between Mazara del Vallo and Agrigento (Lodolo et al., 2019); (2) near the island of Pantelleria (Pantelleria SE, Pantelleria E, Pantelleria SW, Pantelleria Central Bank, Angelia, and Foerstner volcanoes); and (3) north of the island of Linosa (Linosa I, Linosa II, and Linosa II volcanoes). Within the Graham and Terrible volcanic province, the oldest (late Miocene) is the Nameless Bank seamount, which lies ~100 km due east of Pantelleria and ~60 km southwest of Agrigento and rises from a depth of 330-340 m to 80-90 m b.s.l.; the youngest is the Graham Bank seamount, which is located ~45 km southwest of Sciacca and ~70 km northwest of Pantelleria, rises from 330-340 m to 7 m b.s.l., and last erupted in 1831 CE (producing the ephemeral "Ferdinandea Island"; Gemmellaro, 1831; Washington, 1909.)

The island of Pantelleria is by far the larger (~83 km^2) of the two islands and represents the emergent portion of a volcanic edifice that rises 836 m above sea level and about 2200 m above the sea floor within the Pantelleria graben (Calanchi et al., 1989). Most rocks exposed on the island are felsic (trachyte-pantellerite) and younger than the 45.7 ± 1.0 ka pantelleritic Green Tuff, the caldera-forming ignimbrite of the Cinque Denti caldera (Mahood and Hildreth, 1986; Scaillet et al., 2013). The oldest exposed pantelleritic lava on the island has been dated at dated at 324 ± 11 ka (Mahood and Hildreth, 1986), but most of the island is submerged, much older, and most likely primarily basaltic (Fulignati et al., 1997). The oldest documented basalts (~80-120 ka, herein termed "paleo-Pantelleria", following Avanzinelli et al., 2004) are exposed primarily in outcrops along the coast and along the scarp of the Cinque Denti caldera (Mahood and Hildreth, 1986). Younger mafic lavas ("neo-Pantelleria") are found only in the northwestern part of the island and include flows that erupted at ~29 ka from the Cuddie Bruciata, Ferle, and del Monte cinder cones, and at ~10 ka from the Cuddie Rosse cinder cone (Mahood and Hildreth, 1986; Civetta et al., 1998). The most recent volcanic activity occurred ~4 km NW of the island at the submarine (90-100 m b.s.l.) Foerstner volcano on October 17-25, 1891 C.E. (Washington, 1909; Aissi et al., 2015).

The island of Linosa lies ~120 km to the southeast of Pantelleria. Linosa is much smaller (~6 km^2) and represents the emergent portion of a large submarine volcanic complex that rises 196 m above sea level and about 800 m above the sea floor along the SW edge of the Linosa graben (Rossi et al., 1996). Linosa consists entirely of mafic lavas and tuffs that erupted in three stages at 1070 ka (paleo-Linosa), 700 ka (Arena Bianca), and 530 ka (Monte Bandiera) and created several coalescing cinder cone and maar volcanoes (Lanzafame et al., 1994). The paleo-Linosa stage is characterized primarily by hydromagmatic pyroclastic sequences with minor scoria and lava which built maars and cinder cones. The beginning of the Arena Bianca stage was dominated by hydromagmatism followed by eruptions of scoria that built Monte Nero cinder cone and lava flows that created the eastern third of the present-day island. The Monte Bandiera stage also began with hydromagmatic activity that created the Fossa Cappellano maar volcano (and associated Monte Bandiera tuff ring), which was followed by eruptions of scoria and lava that built the Montagna Rossa and Monte Vulcano cinder cones that dominate the western two-thirds of the island (Rossi et al., 1996).

3. Methods and Results

3.1 Methods and materials

Twenty-two samples of mafic lava and scoria were collected from the islands of Pantelleria and Linosa during field trips in 2003, 2006 and 2013, six of which were originally presented in Parker and White (2008) and White et al. (2009). These samples were powdered to -200 mesh in a pre-contaminated shatterbox grinder and were analyzed at Activation

Laboratories, Ontario, for major-elements by ICP-OES and trace-elements (including a full suite of rare earth elements [REE]) by ICP-MS (Code 4Lithoresearch). Whole-rock analyses are presented in Table 1. For the discussion that follows, these analyses are combined with data from literature for a total of 134 analyses of mafic rocks ($SiO_2 \leq 52$ wt% normalized anhydrous); 75 of these include analyses of REE, including 39 from Pantelleria (Civetta et al., 1998; Esperança & Crisci, 1995; Avanzinelli et al., 2004, 2014), 29 from Linosa (Bindi et al., 2002; Di Bella et al., 2008; Avanzinelli et al., 2014), and 7 from various Seamounts (Rotolo et al., 2006; with additional data from Beccaluva, 1981, and Calanchi et al., 1989). Excluded are the Khartibucale hawaiites at Pantelleria, which deserve a separate study; they have trace-element and isotopic signatures significantly different from the rest of the SSRZ basalts, and there are only three known published analyses (Avanzinelli et al., 2004, 2014; White et al., 2009).

3.2 Major-element geochemistry

All samples classify as either basalt or hawaiite (Figure 2a; Le Maitre, 2002), with basalts further classified based on normative mineralogy (assuming $Fe^{3+}/\Sigma Fe = 0.10$) as either alkali basalt (ol+ne-normative) or transitional basalt (ol+hy-normative) on their position in the basalt tetrahedron (Figure 2b; Irvine and Baragar, 1971). Linosa samples from the paleo-Linosa and Monte Bandiera stages are dominated by alkali basalt, with the samples evolving from Ol' (= normative Ol + 0.25Hy) towards normative Ab along the Ol'-Ab join, which divides the "alkali" and "transitional" basalt fields. Linosa samples from the Arena Bianca stage along with most Pantelleria samples classify predominantly as transitional basalts. Mafic lavas and scoriae from both trends are petrographically broadly similar, consisting of lavas with variable amounts of phenocrysts of olivine, clinopyroxene, plagioclase, and magnetite (see Rossi et al., 1996; Civetta

Commentato [DN2]: More for my own understanding that anything else, could you explain what the apostrophe means here? Is it something to do with grouping Mg and Fe together?

et al., 1998; Bindi et al., 2002; Di Bella et al., 2008; and White et al., 2009 for comprehensive descriptions).

Major-element variation diagrams that use wt% MgO as a differentiation index are plotted in Figure 3. Several clear differences can be seen between and within the Pantelleria and Linosa suites. Primitive basalts (MgO > 9 wt%) have not been documented at Pantelleria (max 7.65 wt%, median 5.82 wt% MgO), but have been at Linosa (max 16.35 wt%, median 7.72 wt% MgO). However, the basalts with very high (>14 wt%) MgO at Linosa very likely resulted from the accumulation of olivine (Di Bella et al., 2008). At a given concentration of MgO, Linosa basalts have higher SiO_2 and Al_2O_3, but lower TiO_2 and CaO than Pantelleria basalts (Figures 3a, b, c, e). Elevated values of TiO_2 at a given value of MgO is a characteristic of OIB globally and has been proposed as evidence of a higher degree of mixing of peridotite with recycled MORB lithosphere (Pyrutak and Elliot, 2007). Within the Linosa samples, CaO increases with decreasing to MgO to ~8 wt% after which it decreases, probably indicating fractionation of clinopyroxene and/or plagioclase feldspar at this point. Two distinct trends are observed in plots of MgO versus TiO_2, K_2O, and P_2O_5 (Figures 3b, g, h). The higher-TiO_2, K_2O, and P_2O_5 trend (labelled "A", following Di Bella et al., 2008) includes most of the younger Monte Bandiera (MB) basalts from Linosa and some samples from the older suites; The lower- TiO_2, K_2O, and P_2O_5 trend (labelled "B", following Di Bella et al., 2008) includes most of the older Arena Bianca (AB) basalts from Linosa and some samples from both MB and the older Paleo-Linosa (PL) suites. The younger basalts from Pantelleria (neo-Pantelleria; NP) plot similarly to Trend B with respect to K_2O (but at slightly lower values) and P_2O_5 but with considerably higher TiO_2, whereas the older basalts (paleo-Pantelleria; PP) plot within both trends, but some also with even higher TiO_2 (>3 wt%) and P_2O_5 (>1 wt%) (Civetta et al., 1998). The origin of the two suites at

Commentato [DN3]: Is there any information about these rocks' crystals contents? Values this high suggest to me that these samples contain significant amounts of accommodated olivine.

Linosa has been attributed to fractional crystallization from a similar, hypothetical parental basalt at different pressures, with all geochemical differences due solely to paragenesis and mineral proportions with "Trend-A" representing a younger suite that crystallized at higher pressures (Bindi et al., 2002; Di Bella et al., 2008). In contrast, Civetta et al. (1998) suggested variable degrees of partial melting from a heterogeneous mantle source in addition to fractional crystallization to explain the different basaltic suites at Pantelleria. Haggerty et al. (1994) documented coupled elevated concentrations of Ti and P in eclogitic garnet from the upper mantle, which may support this idea and provide a potential contributing component to the source of these basalts.

Commentato [DN4]: There is a lot made of low-Ti and high-Ti trends in the flood basalt literature. I'm not sure if this relevant here, but it may lend credence to the idea that such variations can come from the mantle.

3.3 Trace-element geochemistry

Trace-element variation diagrams that use wt% MgO as a differentiation index are plotted in Figure 4. As with the major-element geochemistry, trace-element concentrations and ratios show great diversity both between and within the island suites. Within the more primitive Linosa basalts, Sc (Figure 4a) remains fairly constant to ~8 wt% MgO before decreasing, suggesting—like the variation between MgO and CaO—the saturation of clinopyroxene at about this point. Pantelleria basalts are generally higher in Sc at a given concentration of MgO, although many paleo-Pantelleria (PP) basalts plot with the Linosa samples. Nickel (Figure 4b), along with Cr and Co (not shown), demonstrates a constant and linear decrease with MgO indicating fractionation (or accumulation in the case of high-MgO samples) of olivine throughout the suite. Unlike the transition elements, the large-ion lithophile elements (LILE: Rb, Sr, and Ba) and high field-strength elements (HFSE: Zr, Nb, Th) form distinct trends, similar to K_2O and TiO_2, which are labelled in Figures 4c, 4e, 4f, 4g, and 4h but are apparent in Figure 4d as well. Trend-A is again dominated by the Monte Bandiera (MB) lavas from Linosa, and include a few samples

Commentato [DN5]: Or accumulation in the case of high-MgO samples.

from the other Linosan suites as well as some of the paleo-Pantelleria (PP) samples, whereas Trend-B consists of the Arena Bianca (AB) lavas from Linosa as well as a few samples from the other Linosan suites as well as most of the neo-Pantelleria (NP) samples and some of the PP samples. At a given value of MgO, the NP samples demonstrate slightly lower values of Rb, Zr, Nb, and Th than the MB samples.

Representative rare earth element (REE) diagrams (normalized to C1 chondrite; McDonough and Sun, 1995) are presented in Figure 5. AB (Figure 5b) and NP (Figure 5e) display the most internally consistent values, with La_N/Yb_N enrichments of ~7.0 and 9.5 and Sm_N/Yb_N enrichments of ~2.7 and 3.8, respectively. MB (Figure 5c) has a large range of La_N/Yb_N values, but near-constant Sm_N/Yb_N. PL samples (Figure 5a) have similar HREE concentrations, but La_N/Yb_N values either more similar to AB or MB. PP and SEA have the greatest diversity, at least in part because unlike the others they represent discrete volcanic centers that erupted over ~120 ka and 8 Ma, respectively. Several PP samples have La_N/Yb_N and Sm_N/Yb_N ratios similar to NP. Positive Europium anomalies ($Eu/Eu^* = Eu_N/[Sm_N \cdot Gd_N]^{1/2}$) characterize basalts on both islands, with Pantelleria basalts (PP = 1.13 ± 0.17; NP = 1.17 ± 0.09) having a more pronounced anomaly than Linosa basalts (1.06 ± 0.07). Positive Eu anomalies are a common feature in primitive (MgO > 9 wt%) MORB and OIB and have been interpreted as evidence of mixing of DMM with recycled lower continental lithosphere (Niu and O'Hara, 2009; Tang et al., 2015). However, the lack of a negative correlation between Eu/Eu* and radiogenetic lead isotope ratios makes lower continental crust an unlikely component. Alternatively, a positive Eu/Eu* anomaly may simply be due the relative incompatibility of divalent Eu in clinopyroxene compared to trivalent Gd and Sm, coupled with more reducing conditions in the source region which leads to higher $Eu^{2+}/Eu^{3+}$and thus higher Eu/Eu* in the partial melts (Tang et al., 2017).

4.0 Discussion

4.1 Trace element constraints on partial melting and mantle sources.

The isotopic heterogeneity of the mantle has been well-established; however, how this correlates with lithological heterogeneity is much less certain (Zindler and Hart, 1986; Dasgupta et al., 2010; Stracke, 2012). As noted in the Introduction, there is very little variability with respect to Sr and Nd isotopes in the SSRZ basalts (with the exception of the seamounts, which have been strongly affected by chemical alteration). Despite this apparent isotopic homogeneity with respect to Sr-Nd-He, the data clearly show several significant differences with respect to major- and trace-element compositions (and Pb isotopes; Avanzinelli et al., 2014) as well as some key similarities. In this section we investigate these similarities and differences and discuss their constraints on the relative roles of mantle source composition and degree of partial melting in magma generation in the SSRZ.

Commentato [DN6]: I would add a few more citations here. Stracke (2012, Chem Geol) perhaps?

K/Nb and Nb/U ratios for Pantelleria (213.9 ± 38.2 and 48.5 ± 18.1) and Linosa (228.5 ± 22.0 and 46.2 ± 6.0) basalts are similar to global values for OIB (253 ± 71 and 47 ± 10; Hofmann et al., 1986; Halliday et al., 1995; Arevalo et al., 2009) and, combined with Sr-Nd-Pb-O isotope systematics and U-series disequilibrium argue strongly against a significant role for crustal contamination or assimilation in the origin of these basalts (Avanzinelli et al., 2014). Pantelleria and Linosa also have similar incompatible trace element ratios for Th/U (3.3 ± 0.8 and 3.2 ± 1.6), U/Pb (0.59 ± 0.08 and 0.57 ± 0.16), Lu/Hf (0.08 ± 0.01 and 0.07 ± 0.01), and Rb/Sr (0.04 ± 0.01 and 0.05 ± 0.01) which are characteristic of HIMU end-member OIBs (Willbold and Stracke, 2006). Nb/Ta ratios are uniform (Pantelleria: 16.6 ± 1.6; Linosa: 17.1 ± 0.8) and chondritic (17.8; McDonough and Sun, 1995). Typical of OIB, Zr/Hf ratios are mostly superchondritic (>37.1; McDonough and Sun, 1995) and variable, with Pantelleria basalts (42.8 ± 5.8) having generally lower values than Linosa basalts (45.8 ± 2.9), which could reflect smaller degrees of partial melting at Linosa, deeper melting (more residual garnet) at Pantelleria, more eclogite in the source at Pantelleria, or a combination of these (Van Westrenen et al., 2001; Pertermann et al., 2003).

Despite these similarities, there are several systematic differences in other trace element ratios both between and within the islands and seamounts. Ratios of incompatible trace elements (with REE ratios normalized to C1 chondrite; McDonough and Sun, 1995) are presented in Figure 6. La_N/Yb_N is plotted against ppm La in Figure 6a and shows a clear positive slope, strongly suggesting that variable degrees of partial melting are at least partially responsible for compositional variation in these magmas, with the higher values representing smaller melt fractions (cf. Mahood and Baker, 1986). A plot of Sm_N/Yb_N versus La_N/Yb_N (Figure 6b) reveals four sub-groups, which we term **LIN-A** (corresponding to the Linosa Trend-A described above), **LIN-B** (Linosa Trend-B), **PNL-L** (consisting of neo-Pantelleria and geochemically similar paleo-Pantelleria samples), and **PNL-H** (which includes both the high-Ti and P paleo-Pantelleria and the Seamount samples). Although the first three sub-groups may represent consanguineous magmatic suites, PNL-H is clearly an *ad hoc* group consisting of lavas that are unlikely to be related to either each other or the other groups. The lack of collinearity between these sub-groups suggest that although internal variation within them may be attributed to varying degrees of partial melting, the difference in Sm_N/Yb_N at a given value of La_N/Yb_N requires different mantle sources, with the higher Sm_N/Yb_N sub-groups sources being higher in garnet. La_N/Sm_N is a sensitive indicator of partial melting, and therefore its overall positive correlation with La_N/Yb_N (Figure 6c) reinforces support of variation both between and within the groups as attributable to variable melt fractions; however, as with Sm_N/Yb_N, the different trends formed by the Linosa and Pantelleria groups strongly point to compositionally different mantle source regions. This is also seen in a plot of Dy/Dy* (= Dy_N / [$La_N^{4/13} Yb_N^{9/13}$]; Davidson et al., 2013) versus Dy_N/Yb_N (Figure 6d), which reveals three subparallel trends. In this diagram, sub-suite trends with higher Dy_N/Yb_N also indicate a source more enriched in garnet, and the variability within each trend can be attributed to differentiation. The presence of eclogite in the PNL-L source region (and for most of the paleo-Pantelleria samples in PNL-H) may be flagged by the decoupled behavior of Sm_N/Yb_N and Zr/Yb seen in Figure 6e. Experimental work has shown that Zr is much less incompatible and possibly compatible in grossular-rich (eclogitic) garnet compared to pyrope-rich (peridotitic) garnet, whereas D_{Sm}/D_{Yb} is similar in both lithologies (Van Westrenen et al., 2001; Pertermann et al., 2004; Stracke and Bourdon, 2009). Further evidence for this may come from the negative correlation between Sm_N/Yb_N and Rb/La (Figure 6f); Avanzinelli et al. (2014) documented a negative correlation between $^{206}Pb/^{204}Pb$ and Rb/La within the SSRZ basalts and suggested that this ratio may be used a tracer of recycled MORB in the source region following Willbold and Stracke (2006), who demonstrated that (Rb,Ba,K)/La ratios are systematically lower in basalts sourced from HIMU-like mantle. From these observations, we hypothesize: (1) LIN-A and LIN-B are not related by fractional crystallization processes; (2) LIN-A and LIN-B have similar Dy_N/Yb_N and therefore may have similar mantle sources with respect to garnet, with LIN-B derived from a higher melt fraction; (3) the PNL sub-groups cannot be related via fractional crystallization; and (4) PNL-L and PNL-H are either derived from different mantle sources or their differences reflect different degrees of partial melting, with the relatively lower-melt fraction PNL-H sub-suite preserving more of the signal of the more fusible, recycled material (as eclogite).

Spider diagrams of representative analyses from each of the sub-groups ordered by increasing compatibility in oceanic basalts (following Sun and McDonough, 1989) and normalized to depleted MORB mantle (DMM; Salters and Stracke, 2004) are presented in Figure 7. These are plotted with the results of 1% (F = 0.01) non-modal fractional melting of depleted garnet peridotite (GD) and spinel peridotite (SD) using the model parameters of McKenzie and O'Nions (1991, 1995) and trace element partition coefficients of Gibson and Geist (2010). The model results for partial melting of DMM form patterns very similar to those formed by all four sub-groups. Most notably all groups form trends that run subparallel to the model results with excellent fits for the LREE and more compatible elements, consistent with a similar origin by small degrees of partial melting of depleted peridotite in the spinel-garnet transition zone followed by fractional crystallization. However, several notable anomalies require additional explanation: (1) in addition to DMM, the source regions for all four groups require a component enriched in LILE; (2) in addition to the other LILE, the source region beneath Pantelleria must be especially enriched in Ba; (3) a positive P anomaly is present in both Pantelleria groups, and is especially prominent in the PNL-H lavas; (4) PNL suites are characterized by relatively high Ti and low Zr; and (5) the strong variability in PNL-H LILE contents and ratios strongly suggests that several different components must be present in the source region for these diverse magmas which clearly must not be related by either partial melting or fractional crystallization processes. Therefore, we posit: (1) all magmas originate in the spinel-garnet transition zone from a source region dominated by depleted MORB peridotite (Civetta et al., 1998; Neave et al., 2012; Avanzinelli et al., 2014); (2) first-order differences between Pantelleria and

Commentato [DN7]: Maybe highlight how good the fit is for elements of comparable incompatibility to the REEs, anticipating your subsequent comments about LILEs.

Commentato [DN8]: Is there an particular precedent? Or does it mean that P is simply in the wrong place on the spider diagram?

Commentato [WJ-ES9R8]: I reordered this diagram following Sun and McDonough (1988)—the P has moved to the left, so the positive anomaly is less obvious, but it's still present (and elevated above the model results for PNL compared to LIN, anyway.)

Linosa/Seamounts are due to a greater amount of lithologically-enriched and possibly eclogitic material mixed with peridotite in the former (cf. Avanzinelli et al., 2014); (3) differences between the Seamounts, Linosa-A, and Linosa B are due to variable degrees of partial melting, with Seamounts being derived from the smallest melts and Linosa-B being derived from higher degrees of partial melting; (4) differences in degree of partial melting between the Seamounts and Linosa may simply be due to do differences in lithospheric thickness (cf. Niu et al., 2011); (5) compositional diversity within the paleo-Pantelleria suite must reflect the presence of additional diverse components in the mantle source; and (6) compositional homogeneity in the LIN-B and PNL-L is likely due to magma mixing in high-level magma reservoirs, which obfuscates the variability from partial melting seen in LIN-A and heterogeneity observed in PNL-H (e.g., Maclennan, 2008; McGee and Smith, 2016). In most PNL-L samples and some PNL-H samples there is also a positive Ba anomaly which may be the result of a small amount of assimilation of high-Ba alkali feldspar cummulate rock at Pantelleria (White et al., 2012; Wolff, 2017).

4.2 Trace element models of partial melting.

Whole-rock REE concentrations, along with major- and selected trace-element concentrations, were used to model the conditions of partial melting beneath Pantelleria and Linosa by means of the INVMEL program (McKenzie and O'Nions, 1991, 1995, 1998) as modified by White et al. (1992). This program inverts REE geochemical data to find the best-fit relationship between melting conditions (depth to the bottom and top of melting column, degree of partial melting) by running a forward non-modal fractional melting model with the trial parameters, predicting the weighted average composition of the fractional melt, calculating the root-mean square (RMS) error between the predicted and observed calculations, and then

Commentato [DN10]: We should probably comment on the different fusibilities of potential mantle components at some point (probably not here). This is important because low-degrees of melting will preferentially sample lithologically enriched domains (i.e. eclogites etc.). This means that there would have to be significant differences in mantle composition between Linosa and Pantelleria for Pantelleria with its higher-F melting to preserve a greater signal of lithological enrichment in the mantle. Some key reference here would be Hirschmann & Stolper (1996), Kogiso et al. (1998), Shorttle et al. (2014) and Jennings et al (2016).

Commentato [WJ-ES11R10]: Addressed below.

Commentato [DN12]: I know he was my supervisor, but it could be good to back this concept up with a neatly aligned reference. Also, the LIN-A and PNL-H groups potentially represent the groups with the lowest magma fluxes, which would be entirely consistent with them interacting least on their way to the surface.

adjusting the melt depth and degree curve to iteratively minimize the error. After the best-fit parameters producing the least misfit have been calculated, a forward non-modal fractional melting model is run through the remaining major- and trace-element data to evaluate the robustness of fit. Results are considered acceptable if RMS < 1 and the melting curve is relatively smooth. The program also estimates the quantity of olivine and clinopyroxene fractionation (F), and the final melt fraction is adjusted by multiplication by 1/(1-F). The mantle source is set with the ε_{Nd} parameter, which calculates a mixture of depleted MORB mantle (DMM: $\varepsilon_{Nd} = +10$, 0.815 ppm Nd) and bulk silicate earth ("Plume" Mantle, PM: $\varepsilon_{Nd} = 0$, 1.08 ppm Nd) (McKenzie and O'Nions, 1991, 1998). The latter component does not necessarily represent primitive mantle or deep mantle plume material, but serves as a proxy for various enriched components such as recycled oceanic lithosphere well-mixed with peridotite whose compositions are not well-constrained (Gibson and Geist, 2010). Model mineral proportions and chemical composition of DMM and PM sources are from McKenzie and O'Nions (1991, 1995), with the mineral-liquid trace element partition coefficients compiled by Gibson and Geist (2010).

Commentato [DN13]: As far as I can tell from re-reading the McKenzie papers, the only difference between the DMM and PLUME sources is in their trace element contents, not their mineral modes etc. While this is a totally fine simplifying assumption to make, I think it's important to keep it in mind. I guess a key thing to build into the argument below is that simply using a DMM source could not reproduce the chemical trends we observe.

Models were calculated with the top of the melting column fixed at 60 km, consistent with the geophysical evidence for the lithosphere-asthenosphere boundary in the SSRZ (Della Vedova et al., 1995; Civile et al., 2008); variable parameters were the depths of the garnet-spinel transition zone and the bottom of the melting column. It is important to note that the results of these models are relative rather than absolute—for instance for a given mantle source, a model produced with a 60 km top, 70-90 km transition zone, and 100 km bottom provides the exact same results as one produced with a 70 km top, 80-100 km transition zone, and 110 km bottom.

Inversion models for the three subgroups that are plausibly cogenetic (LIN-A, LIN-B, and PNL-L) are presented in Figure 8. Average ε_{Nd} values from Linosa (5.89) were used to set the mantle source region for both LIN-A and LIN-B, and the average ε_{Nd} for neo-Pantelleria (6.01), which correspond to similar mantle sources consisting of 65.5% and 67% DMM respectively. For 60 km thick lithosphere, the best-fit garnet-spinel transition zone was also similar for all three models (~72-92 km), which implies mantle potential temperatures beneath the SSRZ of ~1425°C (Klemme and O'Neill, 2000); however, it is worth repeating that this temperature estimate is coupled with the model parameters—if the lithosphere is set to 63 km and the transition zone is lowered to 75-95 km the results are the same, which suggests a mantle potential temperature of ~1450°C. All models fit the observed REE data well and within 1σ (Figures 8a, b, c), although the observed Eu concentration in PNL-L is noticeably higher. In the forward models (Figures 8d, e, f), the model results also fit the observed major and trace element data well, with a few notable exceptions: Th and Nb are ubiquitously high, but within error; Sr and Zr are low at Linosa, but just barely within 1σ, and below this at Pantelleria. Despite these similarities, the calculated melting curves (Figures 8g, h, j) reveal greater complexity. Calculated depths for both Linosa groups are similar (102 km) and slightly above the intersection of the peridotite mantle solidus (Katz et al., 2003) and the 1425°C adiabat (McKenzie and Bickle, 1988; Putirka et al., 2007) at 103 km, with depth calculated from pressures using the crustal structure and densities of Civile et al. (2008), a mantle density of 3.3 g/cm^3, and a total crustal thickness of 20 km (depth results calculated with a crustal thickness of 25 km instead of 20 km differ by <1 km.). These results suggest that the Linosa basalts are the result of variable degrees of partial melting (1.8% for LIN-A and 3.5% for LIN-B) of similar peridotitic asthenosphere. The presence in each diagram of a small, low-fraction melt "tail" at the base of the melting column may flag the presence of a minor amount lithologically enriched and possibly water-rich material (Gibson and Geist, 2010). This "tail" is much larger and much

Commentato [DN14]: FYI, I obtained similar estimates when doing INVMEL modelling but didn't put them in the paper because I was confused. I think I am still a bit confused, but it seems like slightly elevated potential temperatures are a common and robust feature of continental rift zone magmatism.

Commentato [DN15]: This is also likely to be lithologically enriched and possibly water-rich too. I think McKenzie comments on this in his 1991 and 1995 papers.

more prominent in the PNL-L melting curve, which supports the hypothesis that the mantle source beneath Pantelleria is much more enriched in incompatible trace elements. Likewise, the predicted melting column extends below the peridotite solidus to 110 km at T_P = 1425°C, consistent with early melting of pyroxenitic material, which is more fusible that peridotite and under these conditions would begin melting between 115-130 km (Hirschmann and Stolper, 1996; Kogiso et al., 1998; Pertermann and Hirschmann, 2003). The model for PNL-L also suggests a fraction of partial melting nearly identical to LIN-B (~3.5%); this value is similar to the 3% partial melting suggested by Avanzinelli et al. (2014) on the basis of U-series modelling. The INVMEL model was applied to Pantelleria basalts by Neave et al. (2012), who reported similar results (melting across 100-60 km with the garnet-spinel transition zone between 90-70 km, corresponding to a mantle potential temperature of ~1400°C) but with a much lower melt fraction (~1.7%). This lower value is likely due to the inclusion of high-La/Yb PNL-H samples with the PNL-L basalts in their model.

Commentato [DN16]: Aha. Yes! Hirschmann & Stolper (1996) and Kogiso et al. (1998)

Commentato [DN17]: Here could be good to note that I obtained similar, if slightly lower estimates in my 2012 paper? The approach you have taken is much, much better though. I would also highlight that you are working with a lot more carefully selected compositions. In particular, I think would have lumped your PNL-L and PNL-H groups together. However, I would certainly agree with your assessment that the PNL-H group is not convincingly cogenetic like the PNL-L group may well be.

These model results support the hypotheses described in section 4.1 and the interpretations inscribed in Figure 6. Linosa basalts originate from a common mantle source, and LIN-A and LIN-B can be considered to form collinear trends in each diagram related by partial melting and fractional crystallization. This relationship can be specifically seen in Figure 6d: LIN-A and LIN-B have similar values of $[Dy/Yb]_N$, indicating that their source region is similar with respect to residual garnet, and the higher Dy/Dy* values for LIN-B are the result of higher degrees of partial melting (which does not affect $[Dy/Yb]_N$). The diagonal trends in each group towards lower values of Dy/Dy* and $[Dy/Yb]_N$ are best explained by the effects of fractional crystallization (Davidson et al., 2013). The higher $[Dy/Yb]_N$ and $[Sm/Yb]_N$ values for the Pantelleria basalts indicate the greater influence of residual garnet in the mantle source region, but in this case the so-called “garnet signature” is not the result of lower degrees of partial melting and thicker lithosphere (e.g., Niu et al., 2011) but of a greater amount of lithologically enriched and possibly eclogitic material, which is supported both by the model results and the relatively low values of Zr/Yb and Rb/La (and higher $^{206}Pb/^{204}Pb$) for these basalts. However, many of the seamount data appear to form collinear trends with the Linosa basalts and have higher values of both $[Dy/Yb]_N$ and $[Sm/Yb]_N$; we suggest that for these, the mantle source is the same as Linosa (and may represent the “typical” SSRZ mantle) and are the result of smaller degrees of partial melting owing to thicker lithosphere.

Commentato [DN18]: I am slightly uneasy about describing the enriched source as eclogitic like this. I think there’s a really strong argument that this material must be lithologically enriched, but whether it is in fact eclogitic would be really hard if not impossible to determine. In a paper I’ve just submitted about Iceland I tended to refer to enriched mantle components like this as ‘lithologically enriched’. How about something like ‘lithologically enriched and potentially eclogitic’? I’m happy to go with your final decision, whatever that might be!

4.3 Primary magma compositions and constraints on pressure and temperature of melt generation.

An estimate of the composition of primary basalts is necessary in order to determine the conditions of partial melting in the mantle, such as the source composition, temperature, and pressure/depth of melt segregation. However, every basalt has undergone some degree of fractionation and assimilation prior to eruption and even if assimilation is assumed to be negligible, once the fractionating magma is multiply saturated it becomes very difficult to back-calculate the liquid line of decent (O’Hara, 1968). To do so, of course, first requires the assumption that the rock sample is relatively unweathered and has undergone only olivine fractionation; for this reason, we include only relatively primitive samples characterized by very low (<2 wt%) LOI, relatively high (>9 wt%) MgO, and a lack of a negative Eu anomaly. We also exclude those with very high (>14 wt%) MgO, which could be the result of olivine accumulation. The only samples that fit these criteria are those from Linosa that belong to Linosa-A (see Figures 3, 4). Therefore most of the remainder of the discussion will focus on the

Commentato [DN19]: A classic! Actually the paper I just submitted about Iceland touches on this very point!

origin of the basalts of this sub-group, with inferences made for the origin of the others by comparison.

The composition of the primary magma parental to a basaltic rock may be estimated by iteratively "correcting" it for olivine fractionation until the recalculated basalt has an Mg# that has been experimental determined to be in equilibrium with mantle peridotite with an expected olivine composition of ~Fo_{90} (Lee et al., 2009). Calculated (anhydrous) primary basalts in equilibrium with peridotite with Fo_{90} and $Fe^{3+}/\Sigma Fe = 0.10$ for all samples of that meet the criteria above (n = 25) are very similar, classifying as alkali basalts with $SiO_2 = 46.04 \pm 0.29$ wt%, $TiO_2 = 1.92 \pm 0.07$ wt%, $Al_2O_3 = 13.17 \pm 0.50$ wt%, $Fe_2O_3 = 1.06 \pm 0.03$ wt%, $FeO = 9.92 \pm 0.18$ wt%, $MnO = 0.16 \pm 0.01$, $MgO = 15.65 \pm 0.35$ wt%, $CaO = 8.32 \pm 0.42$ wt%, $Na_2O = 2.59 \pm 0.24$ wt%, and $Ka_2O = 1.13 \pm 0.14$ wt%. Various tests have been proposed to determine the source material for basalts based on their major-element content, but these provide equivocal results. The calculated composition of primary magma for Linosa-A places it within the field of experimental partial melts of peridotite (Dasgupta et al., 2010), although the PRIMELTS3 algorithm places it in the field of partial melts of "pyroxenite" (Herzberg and Asimow, 2008). The Yang and Zhou (2013) test for mantle source composition is also equivocal: the FC3MS (wt% $FeO^T/CaO - 3MgO/SiO_2$) value of the calculated primary basalt (0.27) is within the range for both peridotite (-0.07 ± 0.51) and pyroxenite (0.46 ± 0.96) partial melts. Other major-element ratios purported to flag source compositions for basalts include CaO/Al_2O_3, K_2O/TiO_2 (Jackson and Dasgupta, 2008), and Fe/Mn (Davis et al., 2013) and provide similarly ambiguous results: CaO/Al_2O_3 (0.63 ± 0.04) and K_2O/TiO_2 (0.60 ± 0.08) plot nearest the EM1 component and furthest from the MORB-HIMU array, inconsistent with isotopic evidence; and Fe/Mn for all basalts from both islands is 61.1 ± 5.6 (62.0 ± 0.7) in the model primary magma), which is at the proposed boundary (62) for peridotite- vs. eclogitic-derived melts. Therefore, we suggest that although these tests provide ambiguous results, they also suggest that that unenriched fertile lherzolite is an unlikely source by itself.

Commentato [DN20]: I think a summary sentence would be useful here, even if the “answer” is somewhat unclear. So, it seems to me that, when taken together, these various tests are indicative of a source more enriched than a classical fertile lherzolite, but are equivocal about what it could be.

The olivine-liquid thermobarometer of Lee et al. (2009) provides a weighted average of the temperature and pressure of polybaric melting for the calculated primary basalts of 1463 ± 12°C and 2.69 ± 0.15 GPa; this corresponds to a partial melt fraction of 0.028 ± 0.009 and a mantle potential temperature (T_P) of 1446 ± 14°C (Putirka et al., 2007) (Figure 9). On the basis of thermodynamic modelling, White et al. (2009) suggested that the most primitive Pantelleria basalts may have 0.5-1.0 wt% H_2O; Gioncada and Landi (2010) reported 0.9-1.6 wt% H_2O from a relatively more evolved basalt (5.67 wt% MgO) on Pantelleria. If we assume that Linosa basalts have ~1 wt% H_2O, the calculated primary basalt has major element oxide values only ~1% different from those estimated under anhydrous conditions, but the differences are enough to result in significantly lower model melt fractions (0.018 ± 0.009)—strikingly similar to the value predicted by INVMEL modelling above—as well as lower olivine-liquid temperatures (1435 ± 13°C) and mantle potential temperatures (1415 ± 13°) than those for anhydrous basalts—only pressure (2.62 ± 0.15 GPa) is very similar. Therefore, it might be reasonable to infer mantle potential temperatures in the SSRZ between ~1400-1460°C and average melt segregation depths between 83 and 93 km, with depths calculated from pressures using 20 km thick crust, an average crustal density of 2.70 g/cm^3 (Civile et al., 2008), and mantle density of 3.30 g/cm^3. Model temperatures are higher than those determined for “ambient” MORB mantle (T_P ≈ 1350°C, 0.7-1.7 GPa) and similar to those determined for extension-related intraplate volcanism in the Basin and Range province where the continental lithosphere has been similarly

Commentato [DN21]: Probably worth adding that this approach gives the weighted average P-T of ultimately polybaric melt generation. Both Lee and we know this, but reviewers can be picky! It might be easiest to reword this first sentence to this effect.

Commentato [DN22]: This strikes me as very similar to the results of the INVMEL modelling. It would probably be good to mention this here too.

thinned, such as Owens Valley (southeastern California, USA; ~1425°C, 60-80 km; Lee et al., 2009) and Snow Canyon (southwestern Utah, USA; ~1422°C, 58 km; Plank and Forsythe, 2016).

Commentato [DN23]: I think this is quite an important observation. Maybe we could incorporate a more recent and in depth study of the Basin and Range (Plank & Forsythe, 2016; G3), which also notes elevated temperatures in some locations.

4.4 Thermodynamic models of partial melting and magma evolution.

4.4.1. Partial melting and melt sources

Mantle sources and conditions of partial melting for primary magmas may be semi-quantitatively constrained by comparing the compositions of calculated primary basalts with experimental melts. Shorttle and Maclennan (2011) presented a method to do so whereby the calculated basalt is comparedon an oxide-by-oxide basis to experimental partial melts from an extensive database, with the sum of the absolute differences between them providing a total misfit value (Misfit%). The misfit is then adjusted by adding or subtracting olivine from the original calculated primary magma until the misfit is minimized and the results are reported. A limitation of this method is that experimental results represent partial melts formed at a specific temperature and pressure conditions, whereas natural melts from intraplate settings initially form at the intersection of the solidus and the mantle adiabat and evolve as they isentropically rise to the base of the lithosphere (Niu et al., 2011). In order to account for the great diversity of putative primary melts we modelled the partial melting of various potential mantle lithologies under conditions similar to those beneath the SSRZ. Models were produced with the pMELTS algorigthm (v. 5.6.1; Ghiorso et al., 2002), with model parameters selected based on the results of the INVMEL model and the primary liquid models previously presented . For each potential mantle source composition, isentropic partial melting models were calculated from 3.0 GPa (the upper limit of the pMELTS calibration) to 1.8 GPa (corresponding to the base of ~60 km thick lithosphere) for starting temperatures of 1431, 1456, and 1481°C, corresponding to mantle potential temperatures of 1400, 1425, and 1450°C at 3.0 GPa (McKenzie and Bickle, 1988;

Putirka et al., 2007). Model starting compositions were KLB-1 (fertile lherzolite), KG1 and KG2 (50% and 33% mixtures of average MORB mixed with KLB-1, respectively; Kogiso et al., 1998) and various mixtures of MPY90 and GA1 (MORB pyrolite and average altered oceanic basalt; Yaxley and Green, 1998). All models presented were performed under anhydrous conditions with oxygen fugacities buffered at FMQ; models calculated with more reduced conditions (FMQ-1) provided similar results with slightly higher melt fractions, MgO, FeO, and CaO (~0.003, ~0.21 wt%, ~0.28 wt% and ~0.51 wt% higher respectively), but lower SiO_2, TiO_2, and K_2O (~0.44 wt%, ~0.11 wt% and ~0.02 wt% lower respectively).

For each calculated result, the initial primary basalt (section 4.3) was adjusted by iteratively calculating $K_D(Fe\text{-}Mg)^{ol/liq}$ using the method of Tamura et al. (2000) and then adding or subtracting equilibrium olivine in 0.05 wt% steps following the technique of Herzberg and O'Hara (2002) until the misfit was minimized and the results reported. For each new "best-fit" primary basalt, the average temperature and pressure of melt segregation was then calculated using the geothermobarometer of Lee et al. (2009). These results are presented in Table 2 with selected results also presented in Figure 10. Model results that result in melts with an Mg# < 71 (the highest values recorded in LIN-A excluding samples with evidence of olivine accumulation) or with %F < 0 (indicating an olivine-liquid temperature greater than the initial temperature) are considered unreasonable and inalid. For the remainder, these results show that under anhydrous conditions the consistently best results require low degrees of partial melting (<5%) at higher mantle potential temperatures (1450°C) with a mantle source consisting of between 100 and 62.5% MORB pyrolite mixed with up to 37.5% recycled MORB material. As noted earlier, a slightly hydrous mantle produces very similar results, but with a lower mantle potential temperatures, so 1450°C should be considered a maximum. The pMELTS results confirm the experminetal results of Kogiso et al. (1998), who showed that an addtion of basalt to peridotite results in partial melts higher in FeO and TiO_2 at a given value of MgO. However, TiO_2 is also responsible for the greatest misfit between the model primary basalt and the pMELTS-calculated values. Unlike the pMELTS model, which produced melts up to 1.5 wt% TiO_2, Kogiso et al. (1998) generated melts with TiO_2 > 2.5 wt% for their 33% (KG2) and 50% (KG1) mixtures of basalt with peridotite although their results for partial melting of peridotite (KLB-1) were similar those calculated by pMELTS. Since the behavior of TiO_2 will primarily be controlled by clinopyroxene-melt equilibria, this discrepancy may partly reflect an inadequacy of the clinopyroxene thermodynamic model in the pMELTS program.

4.4.2. Fractional crystallization and magma storage

Pearce (1968) element ratio (PER) diagrams graph ratios of major elements with a conserved, or incompatible, element (e.g., Mg/K, Ca/K) and are presented in Figure 11. PER diagrams are based on the stoichiometry of rock-forming minerals, and slopes of data distributions are equal to major element ratios of minerals lost or gained during differentiation of a cogenetic suite of rocks (Russell and Nicholls, 1988). For example, data plotted with Mg/K on the ordinate and Ca/K on the abscissa will form a linear trend with a slope that varies depending on the fractionating or accumulating assemblage from horizontal for a phase with non-stoichiometric Ca such as olivine to vertical for a phase with non-stoichiometric Mg such as plagioclase. Assemblages with multiple minerals and/or minerals in solid-solution will plot slopes with intermediate values. Diagrams plotting Mg/K versus Al/K (Figure 11a) and Ca/K (Figure 11b) can therefore be used to discriminate between fractionation of olivine (horizontal trends on both diagrams with decreasing Mg/K), clinopyroxene (horizontal trend with Al/K and a positive sloping trend with Ca/K versus Mg/K), and plagioclase (vertical trends on both diagrams).

The two trends ("A" and "B") observed in the major- and trace-element variation diagrams (Figures 3 and 4) are also seen in the PER diagrams (Figure 11). These preclude the possibility of a similar parental magma for the two trends; linking trends A and B by fractional crystallization would require the crystallization of geologically implausible mineral assemblages. PER diagrams show that Trend-A is formed by a paragenetic sequence of olivine to olivine + clinopyroxene to clinopyroxene + plagioclase ± olivine and Trend-B is formed by a continuous sequence of plagioclase + clinopyroxene ± olivine. Samples with Mg/K > 12 have MgO > 14 wt% and are most likely the result of olivine accumulation and have been excluded from this figure. Both trends converge at Mg/K ≈ 4, which corresponds to MgO ≈ 6.5 wt%.

We have modelled these trends using the MELTS algorithm (rhyolite-MELTS v. 1.0.2; Ghiorso et al., 1995; Asimow and Ghiorso, 1998; Gualda et al., 2012), the results of which are superimposed on the data in Figure 10. Trend-A is most successfully modeled as fractional crystallization from the calculated anhydrous primary basalt (section *4.2*) at 0.5 GPa and oxygen fugacities defined by the FMQ buffer. At this pressure, olivine (Fo_{90}) is the liquidus phase at 1432°C, and is joined by clinopyroxene at 1252°C (MgO^{liq} = 8.18 wt%, F = 0.80), magnetite at 1202°C (MgO^{liq} = 5.54 wt%, F = 0.60) and plagioclase at 1192°C (MgO^{liq} = 5.03 wt%, F = 0.55). In contrast, Trend-B is best modelled as the result of fractional crystallization from the most primitive Arena Bianca basalt (LNS11; Bindi et al., 2002) at 0.2 GPa and oxygen fugacities defined by FMQ. At this pressure, olivine (Fo_{82}) is the liquidus phase at 1217°C, and is quickly joined by plagioclase at 1207°C (MgO^{liq} = 7.38 wt%), clinopyroxene at 1178°C (MgO^{liq} = 6.28 wt%), and magnetite at 1142°C (MgO^{liq} = 4.82 wt%). These models are consistent with the conclusions of Bindi et al. (2002), who suggested that the pressure of fractionation at Linosa increased with time based on the clinopyroxene crystal chemistry and structure. Although regarded by most workers to be comprised of attenuated continental crust, a study by Manuella et al. (2015) has suggested an oceanic affinity for the Hyblean-Pelagic basement; these results are more consistent with the former model, and specifically the crustal structure of Civille et al. (2008). Using their model, these pressures would place the 0.5 GPa LIN-A magma chamber at about 17-25 km (approximately the depth of the Moho) and the 0.2 GPa LIN-B magma chamber at about 8-9 km (the top of the crystalline basement / bottom of the sedimentary cover). Pantelleria-L samples form trends subparallel to Linosa-B samples offset to lower Mg/K values for given values of Al/K and Ca/K. The simplest explanation for this is fractional crystallization of these basalts under lower pressures (0.1 GPa, or ~4 km) or under similar pressures but more hydrous conditions (cf. White et al., 2009; Giocanda and Landi, 2009).

5.0 Conclusions

Despite having very similar isotopic characteristics with respect to Sr-Nd-He, there are significant compositional differences both within and between the islands and seamounts with respect to major- and trace-element geochemistry and Pb isotopes (Avanzinelli et al., 2014) that can be attributed to several factors: (1) although broadly similar and dominated by depleted MORB lherzolite, the mantle source is apparently more LILE-enriched and possibly more heterogeneous beneath Pantelleria than Linosa; (2) Linosan mantle may represent the “ambient” mantle in the SSRZ region, as the Seamounts appear to have been derived from a similar source; (3) the fundamental differences between the two trends observed on Linosa (LIN-A and LIN-B) are due to variable degrees of partial melting (~2% and ~3.5%, respectively) as well as different magma storage conditions; (4) Seamounts are likely the result of even lower degrees of partial melting, which may be attributed to magma generation away from the rift grabbens and beneath thicker lithosphere; (5) basalts on Pantelleria are sourced from a mantle similar to Linosa, but with an additional lithologically enriched and possibly eclogitic component. Greater melt productivity at Pantelleria and it's ability to drive felsic magmatism compared to the remainder of the SSRZ and indeed the presence of the island itself may simply be due to the presence of more fusible mantle beneath the island.

Commentato [DN24]: Again, I would probably be tempted to say something a little more tentative: "a lithologically enriched and potentially eclogitic component"

Commentato [DN25]: And it's ability to drive felsic volcanism?

Acknowledgements

This study was funded in part by a grant to the JCW from the University Research Committee and the Rowlett Award from the Society of Foundation Professors at Eastern Kentucky University. JCW would also like to thank Mitchell May and Cassie Simpson for their assistance in the field and computer lab, respectively. DAN was supported by a Presidential Fellowship from the University of Manchester.

References

Aissi, M., Flovere, M., Würtz, M., 2015. Seamounts and seamount-like structures of Sardinia Channel, Strait of Sicily, Ionian Sea, and Adriatic Sea. In: Würtz, M., Rovere, M. (Editors), Atlas of the Mediterranean Seamounts and Seamount-like Structures. International Union for Conservation of Nature (IUCN), Gland, Switzerland and Málaga, Spain, 187-225.

Argnani, A., Torelli, L., 2001. The Pelagian Shelf and its graben system (Italy/Tunisia). In: Ziegler, P.A., Cavazza, W., Robertson, A.H.F. and Crasquin-Soleau, S. (Editors), Peri-Tethys Memoir 6: Peri-Tethyan Rift/Wrench Basins and Passive Margins. Mémoires du Muséum National D'Histoire Naturelle 186, 529-544.

Arevalo, R.,Jr., McDonough, W.F., Luong, M., 2009. The K/U ratio of the silicate Earth: Insights into mantle composition, structure, and thermal evolution. Earth and Planetary Science Letters 278, 361-369, doi: 1016/j.espl.2008.12.023.

Asimow, P.D., Ghiorso, M.S., 1998. Algorighmic modifications extending MELTS to calculated subsolidus phase relations. American Mineralogist 83, 1127-1131.
Avanzinelli, R., Bindi, L., Menchetti, S., Conticelli, S., 2004. Crystallization and genesis of peralkaline magmas from Pantelleria Volcano, Italy: An integrated petrological and crystal-chemical study. Lithos 73, 41-69, doi: 10.1016/j.lithos.2013.10.008.
Avanzinelli, R., Braschi, E., Marchionni, S., Bindi, L., 2014. Mantle melting in within-plate continental settings: Sr-Nd-Pb and U-series isotope constraints in alkali basalts from the Sicily Channel (Pantelleria and Linosa Islands, Southern Italy). Lithos 188, 113-129. doi: 10.1016/j.lithos.2013.008.
Beccaluva, L., Colantoni, P., Di Girolamo, P., Savelli, C., 1981. Upper-Miocene submarine volcanism in the Strait of Sicily (Banco senza Nome). Bulletin of Volcanology 44, 573-581.
Bellani, S., Calore, C., Grassi, S., Squarci, P., 1995. Thermal prospecting in Pantelleria island (Sicily Channel, Italy). World Geothermal Congress, Firenze 1995, 2, 767-770.
Berrino, G., Capuano, P., 1995. Gravity anomalies and structures at the island of Pantelleria. Acta Vulcanologica 7, 19-26.
Bindi, L., Tasselli, F., Olmi, F., Peccerillo, A., Menchetti, S., 2002. Crystal chemistry of clinopyroxenes from Linosa Volcano, Sicily Channel, Italy: implications for modelling the magmatic plumbing system. Mineralogical Magazine 66, 953-968.
Calanchi, N., Colantoni, P., Rossi, P.L., Saitta, M., Serri, G., 1989. The Strait of Sicily continental rift systems: Physiography and petrochemistry of the submarine volcanic centers. Marine Geology 87, 55-83.
Catalano, S., De Guidi, G., Lanzafame, G., Monaco, C., Tortorici, L., 2009. Late Quaternary deformation on the island of Pantelleria: New constraints for the recent tectonic evolution of the Sicily Channel Rift (southern Italy). Journal of Geodynamics 48, 75-82, doi: 10.1016/j.jog.2009.06.005.
Civetta, L., D'Antonio, M., Orsi, G., Tilton, G.R., 1998. The geochemistry of volcanic rocks from Pantelleria Island, Sicily Channel: Petrogenesis and characteristics of the mantle source region. Journal of Petrology 39, 1453-1491.
Civile, D., Lodolo, E., Tortorici, L.Lanzafame, G., Brancolini, G., 2008. Relationships between magmatism and tectonics in a continental rift: The Pantelleira Island region (Sicily Channel, Italy). Marine Geology 251, 32-46.
Coltelli, M., Cavallaro, D., D'Anna, G., D'Alessandro, A., Grassa, F., Mangano, G., Patanè, D., Gresta, S., 2016. Exploring the submarine Graham Bank in the Sicily Channel. Annals of Geophysics 59(2), S0208, doi: 10.4401/ag-6929.
Dasgupta, R., Jackson, M.G., Lee, C.-T.A., 2010. Major element chemistry of ocean island basalts – Conditions of mantle melting and heterogeneity of mantle source. Earth and Planetary Science Letters 289, 377-392, doi: 10.1016/j.espl.2009.11.027.
Davidson, J., Turner, S., Plank, T., 2013. Dy/Dy*: Variations arising from mantle sources and petrogenetic processes. Journal of Petrology 54, 525-537, doi: 10.1093/petrology/egs076.
Davis, F.A., Humayun, M., Hirschmann, M.M., Cooper, R.S., 2013. Experimentally determined mineral/melt partitioning of first-row transition elements (FRTE) during partial melting of peridotite at 3 GPa. Geochimica et Cosmochimica Acta 104, 232-260, doi: 10.1016/j.gca.2012.11.009.

Della Vedova, B., Lucazeau, F., Pasquale, V., Pellis, G., Verdoya, M., 1995. Heat flow in the tectonic provinces crossed by the southern segment of the European Geotraverse. Tectonophysics 244, 57-74.
Di Bella, M., Russo, S., Petrelli, M., Peccerillo, A., 2008. Origin and evolution of the Pleistocene magmatism of Linosa Island (Sicily Channel, Italy). European Journal of Mineralogy 20: 587-601.
Esperança, S., Crisci, G.M., 1995. The island of Pantelleria: A case for the development of DMM-HIMU isotopic compositions in a long-lived extensional setting. Earth and Planetary Science Letters 136, 167-182.
Fouré, E., Allard, P., Jean-Baptiste, P.,Cellura, D., Parello, F., 2012. 3He/4He ratio in olivines from Linosa, Ustica, and Pantelleria Islands (Southern Italy). Journal of Geological Research, doi: 10.1155/2012/723839.
Fulignati, P., Malfitano, G., Sbrana, A., 1997. The Pantelleria caldera geothermal system: Data from the hydrothermal minerals. Journal of Volcanology and Geothermal Research 75, 251-270.
Gemmellaro, C., 1831. Relazione dei fenomeni del nuovo vulcano sorto dal mare fra la costa di Sicilia e l'isola di Pantelleria nel mese di luglio 1831. Atti dell'Accademia Gioenia di Scienze Naturali in Catania 8, 271-298.
Ghiorso, M.S., Sack, R.O., 1995. Chemical mass transfer in magmatic processes. IV. A revised and internally consistent thermodynamic model fo rthe interpolation and extraplation of liquid-solid equilibria in magmatic systems at elevated temperatures and pressures. Contributions to Mineralogy and Petrology 119, 197-212.
Ghiorso, M.S., Hirschmann, M.M., Reiners, P.W., Kress, V.C., 2002. The pMELTS: A revison of MELTS aimed at improving calculation of phase relations and major element partitioning involved in partial melting of the mantle at pressures up to 3 Gpa. Geochemistry, Geophysics, Geosystems 3(5), 10.1029/2001GC000217.
Gibson, S.A., Geist, D., 2010. Geochemical and geophysical estimates of lithospheric thickness variation beheath Galápagos. Earth and Planetary Science Letters 300, 275-286, doi: 10.1016/j.epsl.2010.10.002.
Gioncada, A., Landi, P., 2010. The pre-eruptive volatile contents of recent basaltic and pantelleritic magmas at Pantelleria (Italy). Journal of Volcanology and Geothermal Research 189, 191-201, doi: 10.1016/j.jvolgeores.2009.11.006.
Gualda, G.A.R., Ghiorso, M.S., Lemons, R.V., Carley, T.L., 2012. Rhyolite-MELTS: a modified calibration of MELTS optimized for silica-rich, fluid-bearing magmatic systems. Journal of Petrology 53, 875-890, doi: 10.1093/petrology/egr080.
Haggerty, S.E., Fung, A.T., Burt, D.M., 1994. Apatite, phosphorous and titanium in eclogitic garnet from the upper mantle. Geophysical Research Letters 21, 1699-1702.
Hanyu, T., Kaneoka, I., 1997. The uniform and low $^{3}He/^{4}He$ ratios of HIMU basalts as evidence for their origin as recycled materials. Nature 390, 273-276.
Halliday, A.N., Lee, D.-C., Tommasini, S., Davies, G.R., Paslick, C.R., Fitton, J.G., James, D.E., 1995. Incompatible trace elements in OIB and MORB and source enrichment in the sub-oceanic mangle. Earth and Planetary Science Letters 113, 379-395.
Herzberg, C., Asimow, P.D., 2008. PRIMELT3 MEGA.XLSM software for primary magma calculation: Peridotite primary magma MgO contents from the liquidus to the solidus. Geochemistry, Geophysics, Geosystems 16, 563-578, doi: 10.1002/2014GC00563.

Herzberg, C., O'Hara, M.J., 2002. Plue-associated ultramafic magmas of Phanerozoic age. Journal of Petrology 43, 1857-1883.
Hirschmann, M.M., Stolper, E.M., 1996. A possible role for garnet pyroxenite in the origin of the "garnet signature" in MORB. Contributions to Mineralogy and Petrology 124, 185-208.
Hofmann, A.W., Jochum, K.P., Seufert, M., White, W.M., 1986. Nb and Pb in oceanic basalts: new constraints on mantle evolution. Earth and Planetary Science Letters 79, 33-45.
Irvine, T.N., Baragar, W.R.A., 1971. A guide to the chemical classification of the common volcanic rocks. Canadian Journal of Earth Sciences 8, 523-548.
Jackson, M.G., Dasgupta, R., 2008. Compositions of HIMU, EM1, and EM2 from global trends between radiogenic isotopes and major elements in oceanic island basalts. Earth and Planetary Science Letters 276, 175-186, doi: 10.1016/j.espl.2008.09.023.
Katz, R.F., Spiegelman, M., Langmuir, C.H., 2003. A new parameterization of hydrous manlte melting. Geochemistry Geophysics Geosystems 4(9), 1073, doi: 10.1029/2002GC000433.
Klemme, S., O'Neil, H.StC., 2000. The near-solidus transition from garnet lherzolite to spinel lherzolite. Contributions to Mineralogy and Petrology 138, 237-248.
Kogiso, T., Hirose, K., Takahashi, E., 1998. Melting experiments on homogenous mixtures of peridotitee and basalt: application to the genesis of ocean island basalts. Earth and Planetary Science Letters 162, 45-61.
Lanzafame, G., Rossi, P.L., Tranne, C.A., Lanti, E., 1994. Carta geologica dell'isola di Linosa. 1:5000. Società Elaborazioni Cartografiche, Firenze.
Lee, C.-T.A., Luffi, P., Plank, T., Dalton, H., Leeman, W.P., 2009. Constraints on the depths and temperatures of basaltic magma generation on Earth and other terrestrial planets using new thermobarometers for mafic magmas. Earth and Planetary Science Letters 279, 20-33, doi: 10.1016/j.espl.2008.12.020.
Le Maitre, R.W. (Editor), 2002. Igneous rocks, a classification and glossary of terms: Recommendations of the International Union of Geological Sciences Subcomission on the Systematics of Igneous Rocks, 2nd Ed. Cambridge University Press, 236 p.
Lodolo, E., Zampa, L., Civile, D., 2019. The Graham and Terrible volcanic province (NW Sicilian Channel): gravimetric constraints for the magmatic manifestations. Bulletin of Volcanology 81, 17, doi:10.1007/s00445-019-1274-0.
Maclennan, J., 2008. Lead isotope variability in olivine-hosted melt inclusions from Iceland. Geochimica et Cosmochimia Acta 72, 4159-4176.
Mahood, G.A., Baker, D.R., 1986. Experimental constraints on depths of fractionation of mildly alkalic basalts and associated felsic rocks: Pantelleria, Strait of Sicily. Contributions to Mineralogy and Petrology 93, 251-264.
Mahood, G.A., Hildreth, W., 1986. Geology of the peralkaline volcano at Pantelleria, Strait of Sicily. Bulletin of Volcanology 48, 143-172.
Manuella, F.C., Scribano, V., Carbone, S., Brancato, A., 2015. The Hyblean xenolith suite (Sicily): an unexpected legacy of the Ionian-Tethys realm. International Journal of Earth Science 104, 1317-1336, doi: 10.1007/s00531-1151-9.
McDonough, W.F., Sun, S.-s., 1995. The composition of the Earth. Chemical Geology 120, 223-253.
McGee, L.E., Smith, I.E.M., Interpreting chemical compositions of small scale basaltic systems: A review. Journal of Volcanology and Geothermal Research 325, 45-60, doi: 10.1016/j.volgeores.2016.06.007.

McKenzie, D., Bickle, M.J., 1988. The volume and composition of melt generated by extension of the lithosphere. Journal of Petrology 29, 625-679.
McKenzie, D., O'Nions, R.K., 1991. Partial melt distributions from inverstion of rare earth element concentrations. Journal of Petrology 32, 1021-1091, doi: 10.1093/petrology/32.5.1021.
McKenzie, D., O'Nions, R.K., 1995. The source regions of ocean island basalts. Journal of Petrology 36, 133-159.
McKenzie, D., O'Nions, R.K., 1998. Melt production beneath oceanic islands. Physics of the Earth and Planetary Interiors 107, 143-182.
Niu, Y., O'Hara, M.J., 2009. MORB mantle hosts the missing Eu (Sr, Nb, Ta, and Ti) in the continental crust: New perspectives on crustal growth, crust-mantle differentiation and chemical signature of the oceanic upper mantle. Lithos 112, 1-17, doi: 10.1016/j.lithos.2008.12.009.
Niu, Y., Wilson, M., Humphrey, E.R., and O'Hara, M.J., 2011. The origin of intra-plate ocean island basalts (OIB): the lid effect and its geodynamic implications. Journal of Petrology 52, 1443-1468, doi: 10.1093/petrology/egr030.
Neave, D.A., Fabbro, G., Herd, R.A., Petrone, C.M., Edmonds, M., 2012. Melting, differentiation and degassing at the Pantelleria Volcano, Italy. Journal of Petrology 53, 637-663.
Parello, F., Allard, P., D'Alessandro, W., Federico, C., Jean-Baptiste, P., Catani, O., 2000. Isotope geochemistry of Pantelleria volcanic fluids, Sicily Channel rift: a mantle volatile end-member for volcanism in southern Europe. Earth and Planetary Science Letters 180, 325-339.
Parker, D.F., White, J.C., 2008. Large-scale alkalic magmatism associated with the Buckhorn caldera, Trans-Pecos Texas, USA: Comparison with Pantelleria, Italy. Bulletin of Volcanology 70, 403-415.
Pearce, T.H., 1968. A contribution to the theory of variation diagrams. Contributions to Mineralogy and Petrology 19, 142-157.
Pertermann, M., Hirschmann, M.M., 2003. Partial melting experiments on a MORB-like pyroxenite between 2 and 3 GPa: Constraints on the presence of pyroxenite in basalt source retions from solidus location and melting rate. Journal of Geophysical Research 108, no. B2, 2125, doi: 10.1029/2000JB000118.
Pertermann, M., Hirschmann, M.M., Hametner, K, Günther, D., Schmidt, M.W., 2004. Experimental determination of trace element partitioning between garnet and silica-rich liquid during anhydrous melting of MORB-like eclogite. Geochemistry Geophysics Geosystems, 5(5), Q05A01, doi: 10.1029/2003/GC000638.
Prytulak, J., Elliot, T., 2007. TiO_2 enrichment in ocean island basalts. Earth and Planetary Science Letters 263, 388-403, doi: 10.1016/j.epsl.2007.09.015.
Putirka, K.D., Perfit, M., Ryerson, F.J., Jackson, M.G., 2007. Ambient and excess mantle termperatures, olivine thermometry, and active vs. passive upwelling. Chemical Geology, 241, 177-206, doi: 10.1016/j.chemgeo.2007.01.014.
Rossi, P.L., Tranne, C.A., Calanchi, N., Lanti, E., 1996. Geology, stratigraphy and volcanological evolution of the island of Linosa (Sicily Channel). Acta Vulcanologica 8, 73-90.
Rotolo, S.G., Castorina, F., Cellura, D., Pompilio, M., 2006. Petrology and geochemistry of submarine volcanism in the Sicily Channel rift. Journal of Geology 114, 355-365.

Russell, J.K., Nicholls, J., 1988. Analysis of petrologic hypotheses with Pearce element ratios. Contributions to Mineralogy and Petrology 99, 25-35.
Salters, V.J.M., Stracke, A., 2004. Composition of depleted mantle. Geochemistry, Geophysics, Geosystems 5(5), Q05004, doi:10.1029/2003GC000597.
Scaillet, S., Vita-Scaillet, G., Rotolo, S.G., 2013. Millennial-scale phase relationships between ice-core and Mediterranean marine records: insights from high-precision $^{40}Ar/^{39}Ar$ dating of the Green Tuff of Pantelleria, Sicily Strait. Quaternary Science Reviews 78, 141-154.
Shorttle, O., Maclennan, J., 2011. Compositional trends of Icelandic basalts: Implications for short-length scale lithological heterogeneity in mantle plumes. Geochemistry Geophysics Geosystems 12(11), Q11009, doi: 10.1029/2011GC003748.
Stracke, A., Bourdon, B., 2009. The importance of melt extraction for tracing mantle heterogeneity. Geochimica et Cosmochimica Acta 73, 218-238, doi: 10.1016/j.gca.2008.10.015.
Stracke, A., 2012. Earth's homegenous mantle: A product of convection-driven interacton between crust and mantle. Chemical Geology 330-331, 274-299, doi: 10.1016/j.chemgeo.2012.08.007.
Sun, S.-s., McDonough,W.F., 1989. Chemical and isotopic systematics of oceanic basalts: implications for mantle composition and processes. Geological Society, London, Special Publications 42, 313-345, doi: 10.1144/GSL.SP.1989.042.01.19.
Tamura,Y., Yuhara, M., Ishii, T., 2000. Primary arc basalts from Daisen Volcano, Japan: equilibrium crystal fractionation versus disequilibrium fractionation during super-cooling. Journal of Petrology 41, 431-448.
Tang, M., Rudnick, R.L., McDonough, W.F., Gaschnig, R.M., Huang, Y., 2015. Europium anomalies constrain the mass of recycled lower continental crust. Geology 43, 703-706, doi: 10.1130/G36641.1.
Tang, M., McDonough, W.F., Ash, R.D., 2017. Europium and strontium anomalies in the MORB source mantle. Geochimica et Cosmochimica Acta 197, 132-141, doi: 10.1016/j.gca.2016.10.025.
van Westrenen, W., Blundy, J.D., Wood, B.J., 2001. High field strength element / rare earth element fractionation during partial melting in the presence of garnet: Implications for identification of mantle heterogeneities. Geochemistry Geophysics Geosystems, doi: 10.1029/2000GC000133.
Washington, H.S., 1909. Art. VIII.—The submarine eruptions of 1831 and 1891 near Pantelleria. American Journal of Science 27, 131-150, n. 158, doi: 10.2475/ajs.s4-27.158.131.
White, R.S., McKenzie, D., O'Nions, R.K., 1992. Oceanic crustal thickness from seismic measurements and rare earth element inversions. Journal of Geophysical Research 97, 19683-19715.
White, J.C., Parker, D.F., Ren, M., 2009. The origin of trachyte and pantellerite from Pantelleria, Italy: Insights from major element, trace element, and thermodynamic modelling. Journal of Volcanology and Geothermal Research 179, 33-55.
White, J.C., Espejel-García, V.V., Anthony, E.Y., Omenda, P., 2012. Open system evolution of peralkaline trachyte and phonolite from the Suswa volcano, Kenya rift. Lithos 152, 84-104.
Wolff, J.A., 2017. On the syenite-trachyte problem. Geology 45, 1067-1070, doi: 10.1130/G39415.1.

Willbold, M., Stracke, A., 2006. Trace element composition of mantle end-members: Implications for recycling of oceanic and upper and lower continental crust. Geochemistry Geophysics Geosystems 7(4), Q04004, doi: 10.1029/2005GC001005.

Yang, Z.-F., Zhou, J.-H., 2013. Can we identify source lithology of basalt? Scientific Reports 3, 1856, doi: 10/1038/srep01856.

Yaxley, G.M., Green, D.H., 1998. Reactions between eclogite and peridotite: mantle refertilisation by subduction of oceanic crust. Schweizerische Mineralogische und Petrographische Mitteilungen 78, 243-255

Zindler, A., Hart, S., 1986. Chemical geodynamics. Annual Review of Earth and Planetary Sciences 14, 493-571.

FIGURE CAPTIONS

Figure 1. Schematic structural map of the Strait of Sicily. PT: Pantelleria trough; MT, Malta trough; GB, Graham Bank. Used with permission from Catalano et al. (2009).

Figure 2. (a) Total-alkali versus silica (TAS) diagram for the classification of volcanic rocks (Le Maitre, 2002). (b) Basalt tetrahedron projected from clinopyroxene: Q' = Q + 0.4Ab + 0.25Hy; Ol' = Ol + 0.75Hy; Ne' = Ne + 0.6Ab (Irvine and Baragar, 1971). Alkali basalts plot below the plane of critical silica undersaturation (solid line); transitional basalts plot below the plane of critical silica saturation (dashed line). Units: PL, Paleo-Linosa; AB, Arena Bianca (Linosa); MB, Monte Bandiera (Linosa); PP, Paleo-Pantelleria; NP, Neo-Pantelleria; SEA, Semounts.

Figure 3. Major-element variation diagrams that use MgO as the differentiation index. Dashed lines illustrate the two major trends (see text for details.) Units: PL, Paleo-Linosa; AB, Arena Bianca (Linosa); MB, Monte Bandiera (Linosa); PP, Paleo-Pantelleria; NP, Neo-Pantelleria; SEA, Seamounts. Trends labeled A and B correspond to the Linosa trends of Di Bella et al. (2008).

Figure 4. Trace-element variation diagrams that use MgO as the differentiation index. Units: PL, Paleo-Linosa; AB, Arena Bianca (Linosa); MB, Monte Bandiera (Linosa); PP, Paleo-Pantelleria; NP, Neo-Pantelleria; SEA, Seamounts Trends labeled A and B correspond to the Linosa trends of Di Bella et al. (2008).

Figure 5. Representative rare-earth element diagrams (normalized to C1 Chondrite; McDonough and Sun, 1995). In each graph, n = the total number of analyses in the dataset. REE ratios are reported either as a range or averages with standard deviation.

Figure 6. Trace element ratio diagrams, with REE ratios normalized to C1 Chondrite (McDonough and Sun, 1995). Units: PL, Paleo-Linosa; AB, Arena Bianca (Linosa); MB, Monte Bandiera (Linosa); PP, Paleo-Pantelleria; NP, Neo-Pantelleria; SEA, Seamounts. Identified geochemical groups are labelled, as are the interpretations of the variation as discussed in the text.

Figure 7. Spiderdiagrams of representative samples (normalized to depleted MORB mantle [DMM]; Salters and Stracke, 2004) for each of the geochemical groups identified in Figure 6. Values in parenthesis are wt% MgO of each sample. The dotted lines superimposed on each represent model non-modal fractional melts (F = 0.01) of DMM for garnet peridotite (GD) and spinel peridotite (SD) (see text for details).

Figure 8. Results of rare-earth element inverse modelling (a, b, c), major- and trace-element forward model predictions (d, e, f), and calculated melting curves (g, h, j) for LIN-A, LIN-B, and PNL-L.

Figure 9. FractionatePT3 (Lee et al., 2009) model results for Linosa-A magmas. LAB: lithosphere-asthenosphere boundary. Gt-In, Sp-Out: garnet-spinel transition zone (Klemme and

O'Neil, 2000). Dry fertile lherzolite solidus from Katz et al. (2003). Adiabats calculated following McKenzie and Bickle (1988) and Putirka et al. (2007).

Figure 10. Compositions for selected pMELTS models plotted versus compositions of LIN-A basalts and the average model primary basalt compositions (the symbol width corresonds to approximately 1σ, as shown in Figure 10a). The MELTS model for fractional crystallization of this primary basalt to produce the LIN-A magmas is also shown (see also Figure 11.)

Figure 11. Pearce (1968) element ratios plotted with the results of MELTS (rhyolilte-MELTS v.1.0; Gualda et al., 2012) models of fractional crystallization at 0.2 and 0.5 GPa.

Fig 1

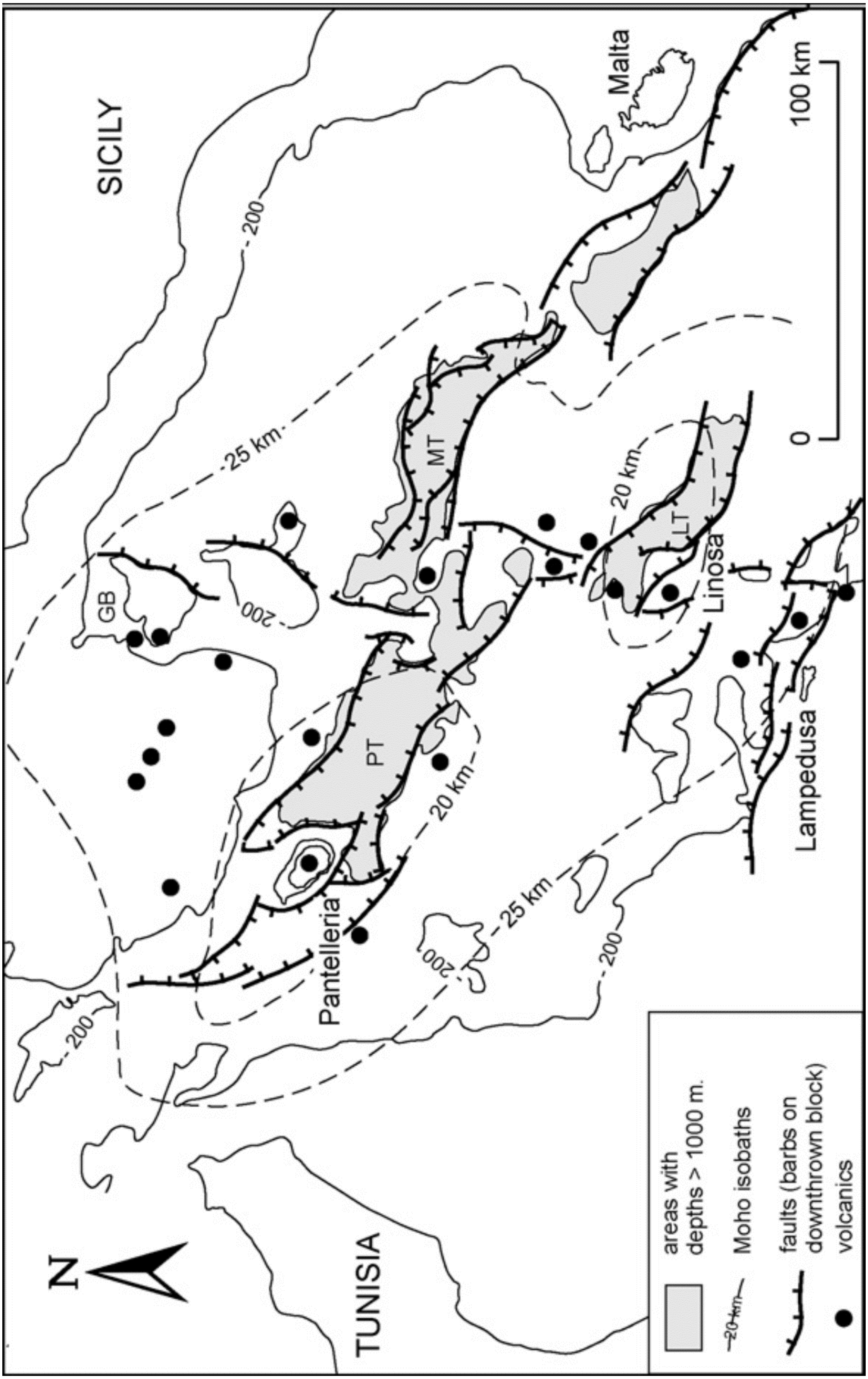
SICILY
TUNISIA
Malta
Pantelleria
Linosa
Lampedusa
GB
PT
MT
LT
200
25 km
20 km
0
100 km
N
areas with depths > 1000 m.
20 km
Moho isobaths
faults (barbs on downthrown block)
volcanics

Fig 2

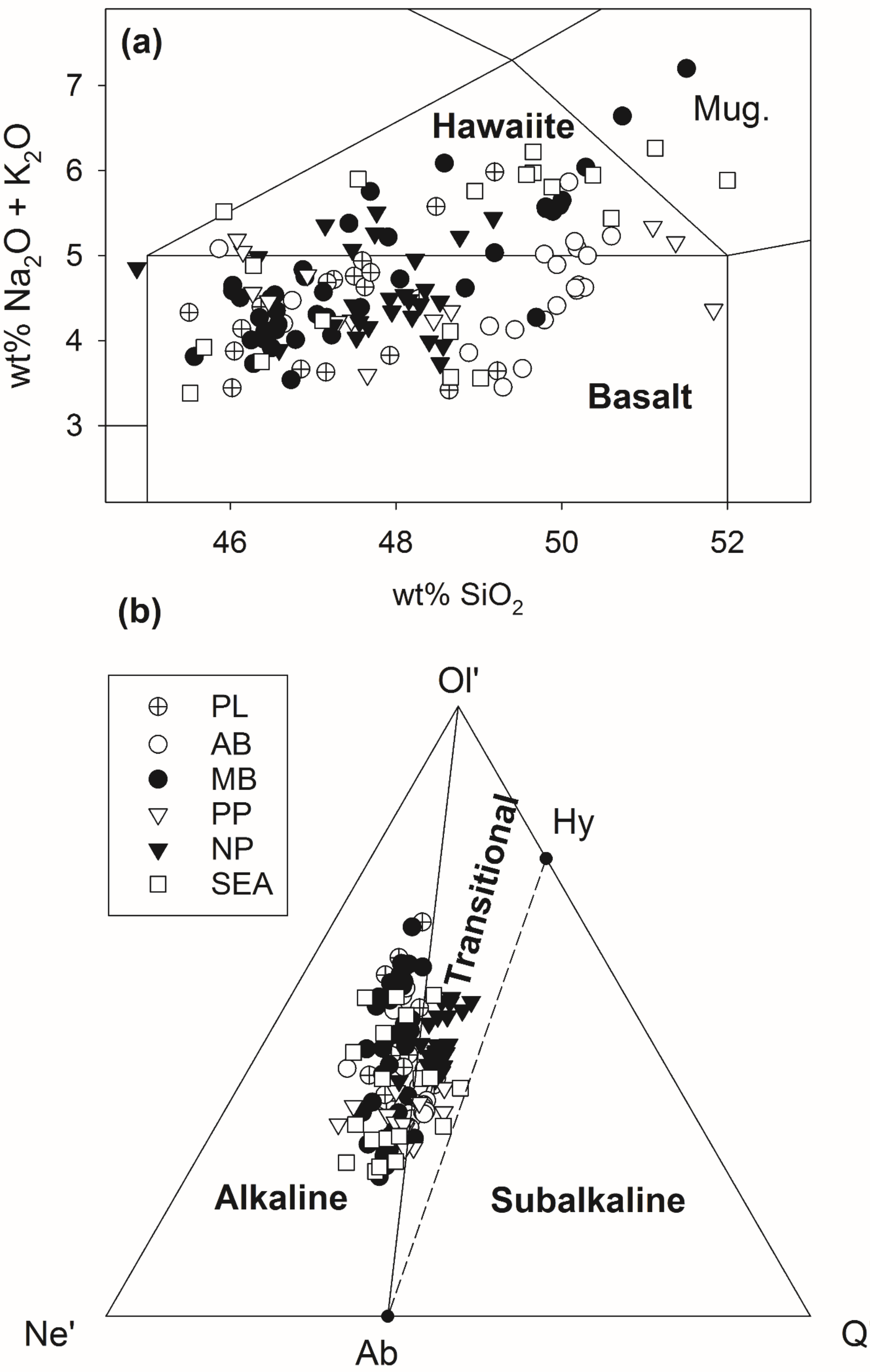

(a)
Hawaiite
Mug.
Basalt
wt% Na2O + K2O
wt% SiO2
3
4
5
6
7
46
48
50
52
(b)
PL
AB
MB
PP
NP
SEA
Ol'
Hy
Transitional
Alkaline
Subalkaline
Ne'
Ab
Q'

Fig 3

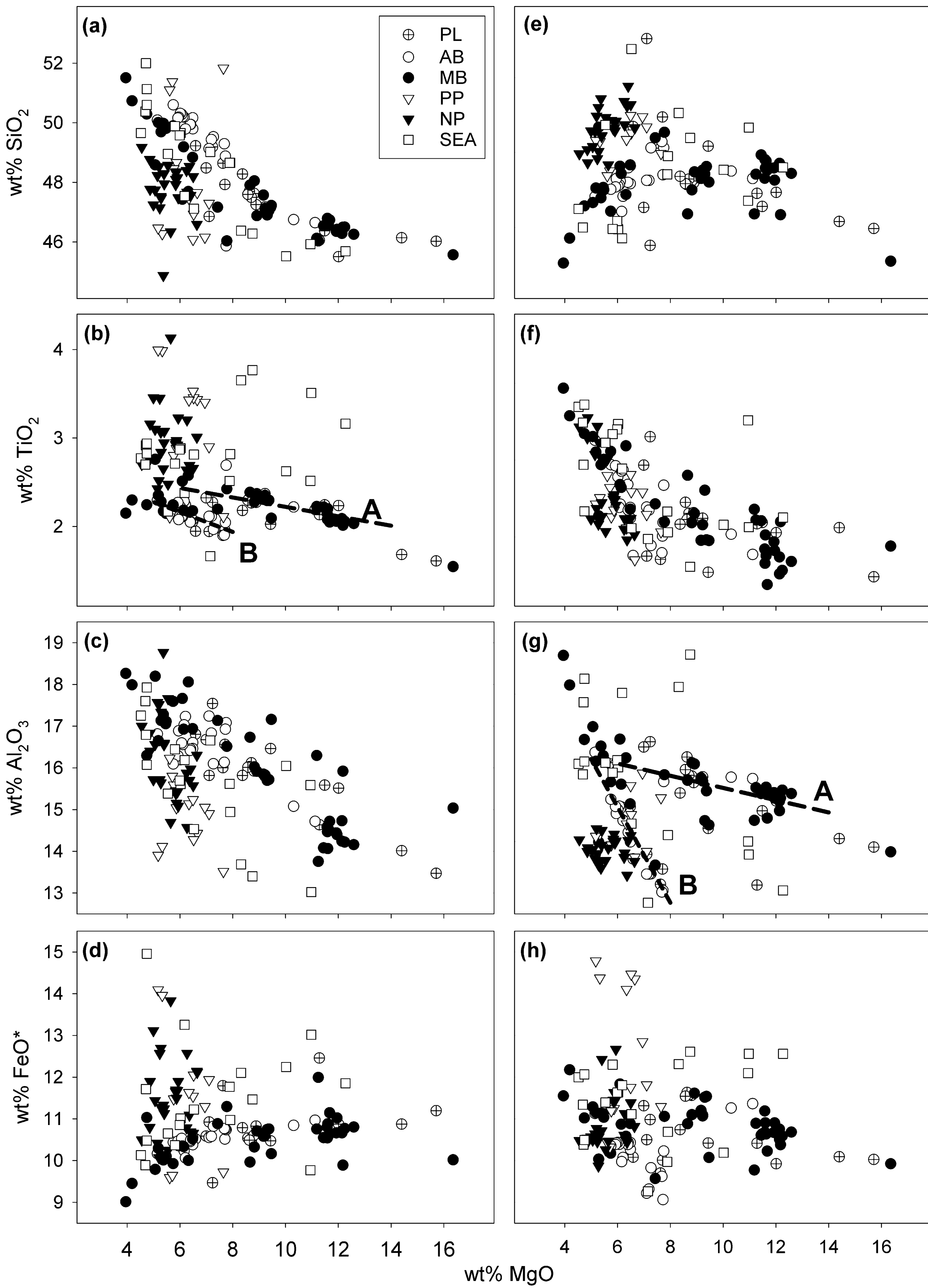

(a)
(b)
(c)
(d)
(e)
(f)
(g)
(h)
PL
AB
MB
PP
NP
SEA
wt% SiO_2
wt% TiO_2
wt% Al_2O_3
wt% FeO*
wt% CaO
wt% Na_2O
wt% K_2O
wt% P_2O_5
A
B
A
B
wt% MgO

Fig 4

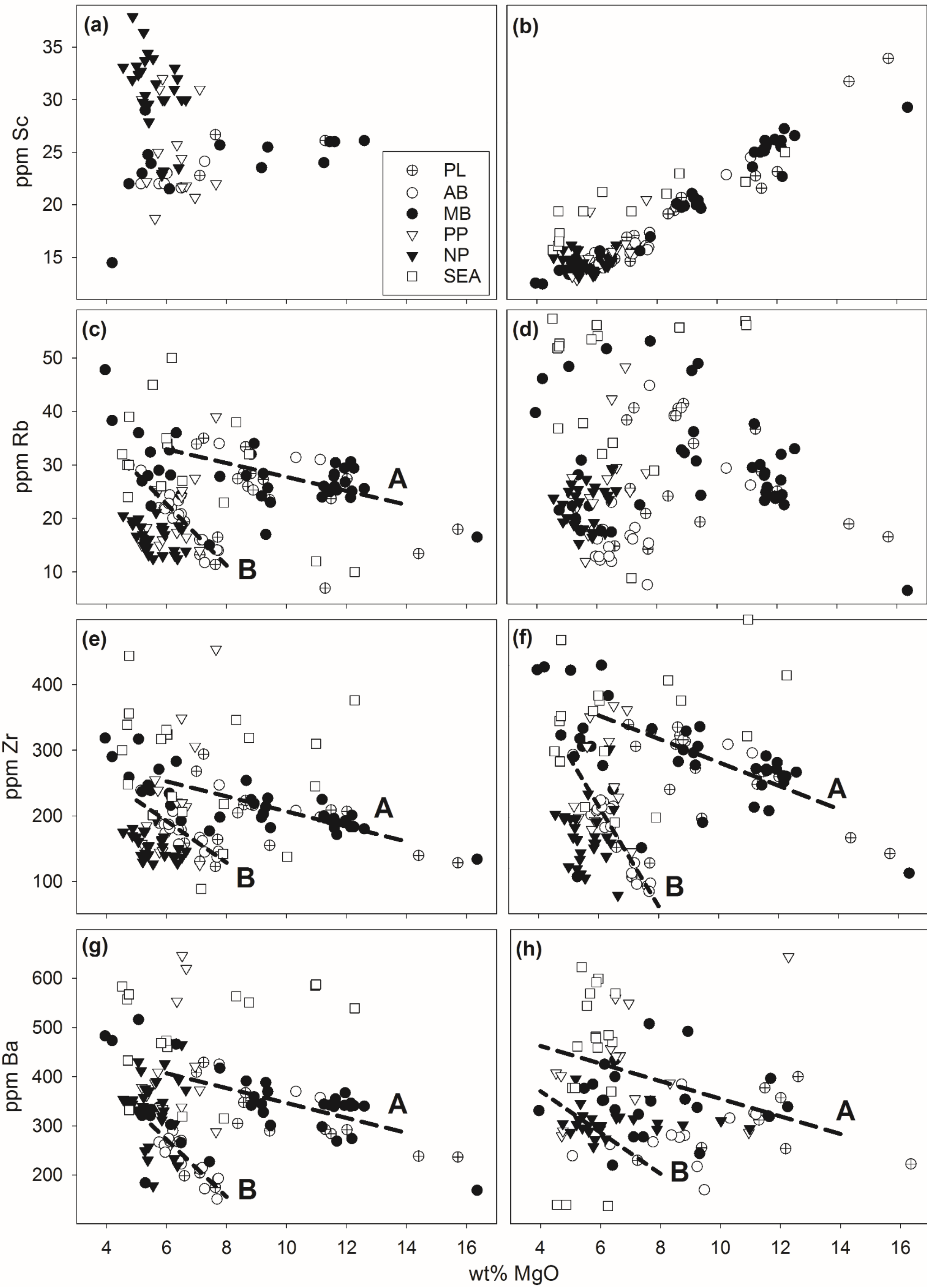

(a)
(b)
(c)
(d)
(e)
(f)
(g)
(h)
ppm Sc
ppm Ni
ppm Rb
ppm Sr
ppm Zr
ppm Nb
ppm Ba
ppm La
PL
AB
MB
PP
NP
SEA
A
B
wt% MgO

Fig 5

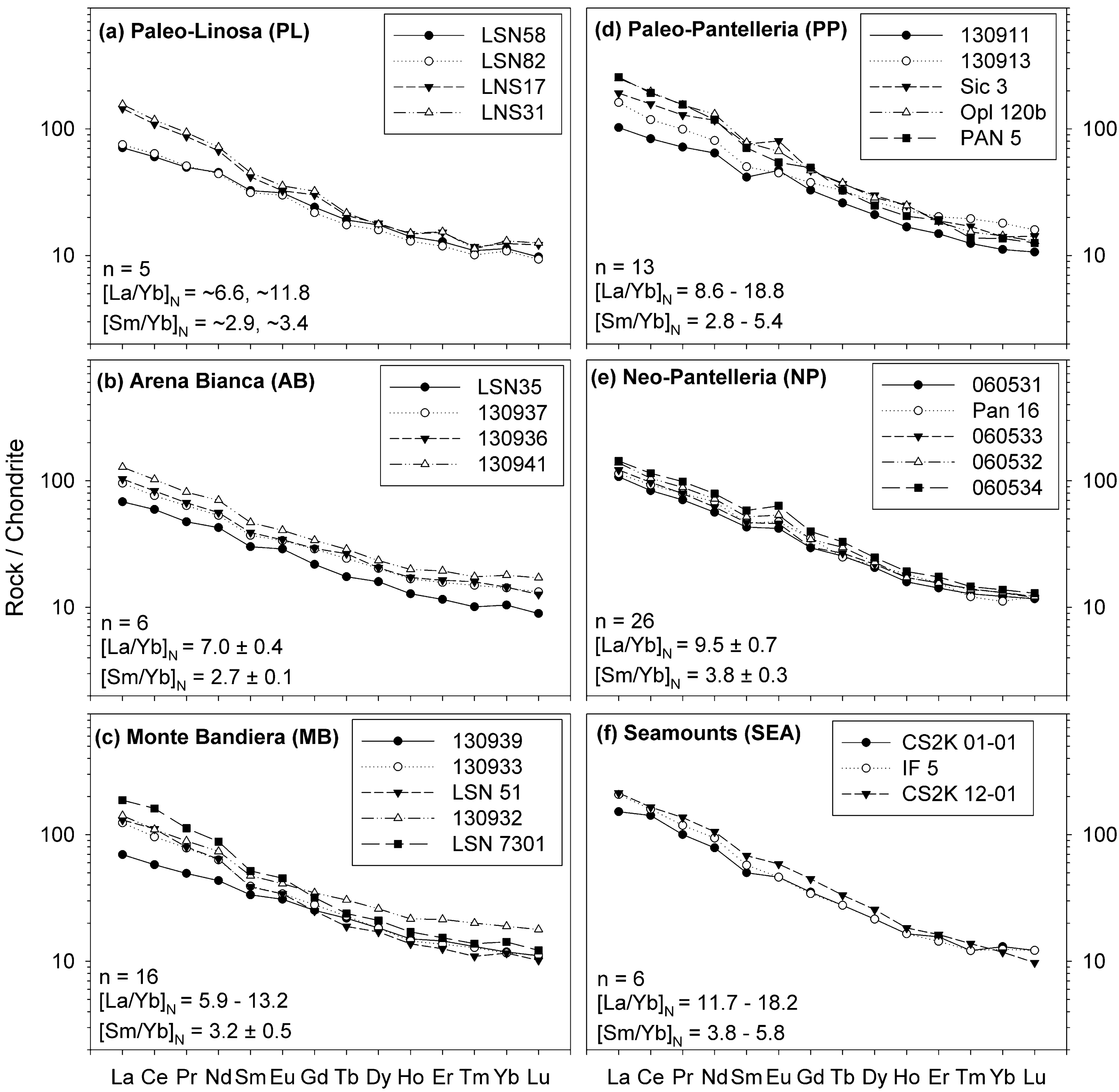

(a) Paleo-Linosa (PL)
LSN58
LSN82
LNS17
LNS31
n = 5
[La/Yb]N = ~6.6, ~11.8
[Sm/Yb]N = ~2.9, ~3.4
(b) Arena Bianca (AB)
LSN35
130937
130936
130941
n = 6
[La/Yb]N = 7.0 ± 0.4
[Sm/Yb]N = 2.7 ± 0.1
(c) Monte Bandiera (MB)
130939
130933
LSN 51
130932
LSN 7301
n = 16
[La/Yb]N = 5.9 - 13.2
[Sm/Yb]N = 3.2 ± 0.5
(d) Paleo-Pantelleria (PP)
130911
130913
Sic 3
Opl 120b
PAN 5
n = 13
[La/Yb]N = 8.6 - 18.8
[Sm/Yb]N = 2.8 - 5.4
(e) Neo-Pantelleria (NP)
060531
Pan 16
060533
060532
060534
n = 26
[La/Yb]N = 9.5 ± 0.7
[Sm/Yb]N = 3.8 ± 0.3
(f) Seamounts (SEA)
CS2K 01-01
IF 5
CS2K 12-01
n = 6
[La/Yb]N = 11.7 - 18.2
[Sm/Yb]N = 3.8 - 5.8
Rock / Chondrite
100
10
La Ce Pr Nd Sm Eu Gd Tb Dy Ho Er Tm Yb Lu

Fig 6

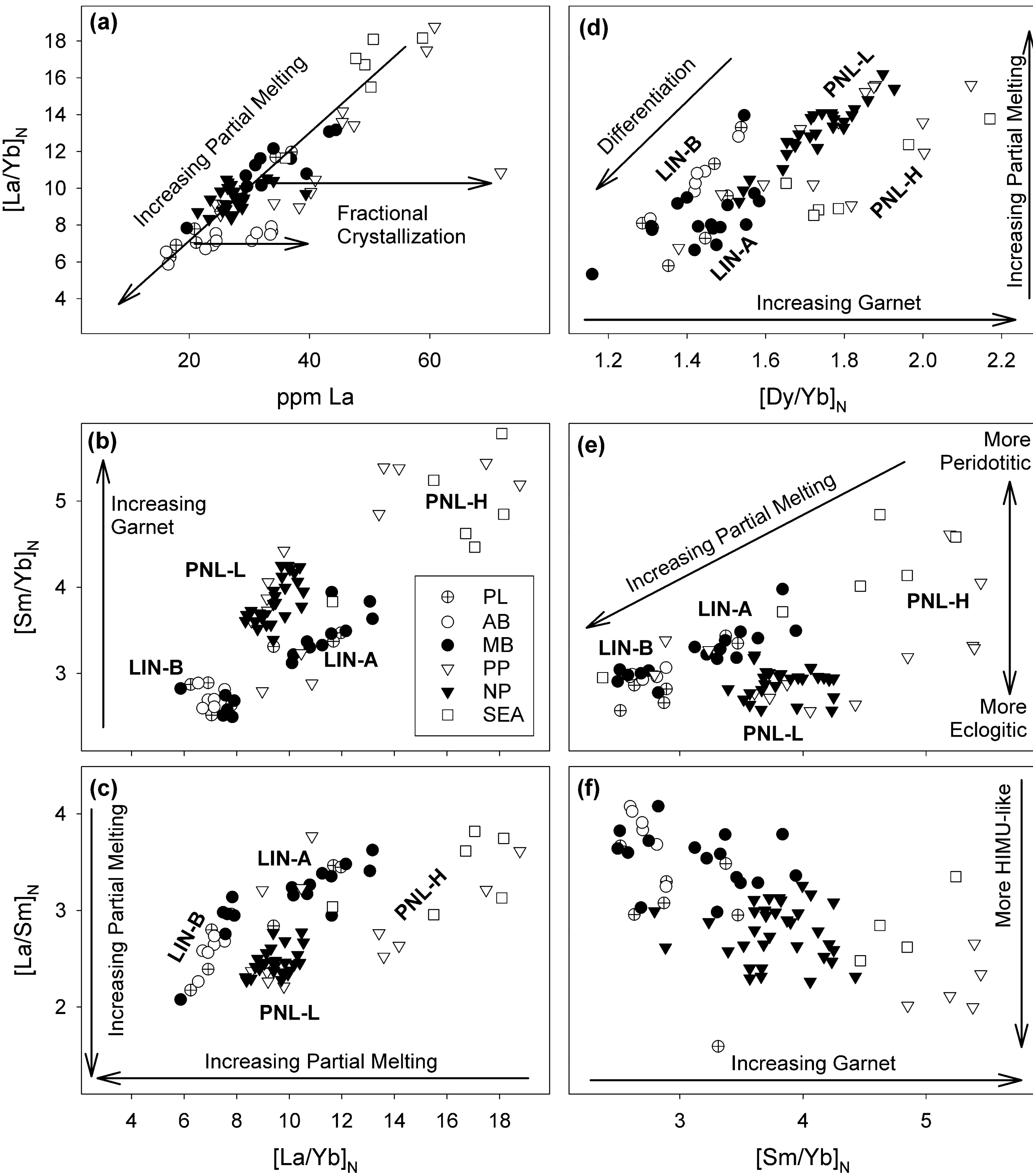

(a)
Increasing Partial Melting
Fractional Crystallization
[La/Yb]N
ppm La
(d)
Differentiation
LIN-B
LIN-A
PNL-L
PNL-H
Increasing Partial Melting
Increasing Garnet
Dy/Dy*
[Dy/Yb]N
(b)
Increasing Garnet
PNL-H
PNL-L
LIN-B
LIN-A
PL
AB
MB
PP
NP
SEA
[Sm/Yb]N
(e)
Increasing Partial Melting
More Peridotitic
More Eclogitic
LIN-A
LIN-B
PNL-H
PNL-L
Zr/Yb
(c)
Increasing Partial Melting
LIN-A
LIN-B
PNL-H
PNL-L
Increasing Partial Melting
[La/Sm]N
[La/Yb]N
(f)
More HIMU-like
Increasing Garnet
Rb/La
[Sm/Yb]N

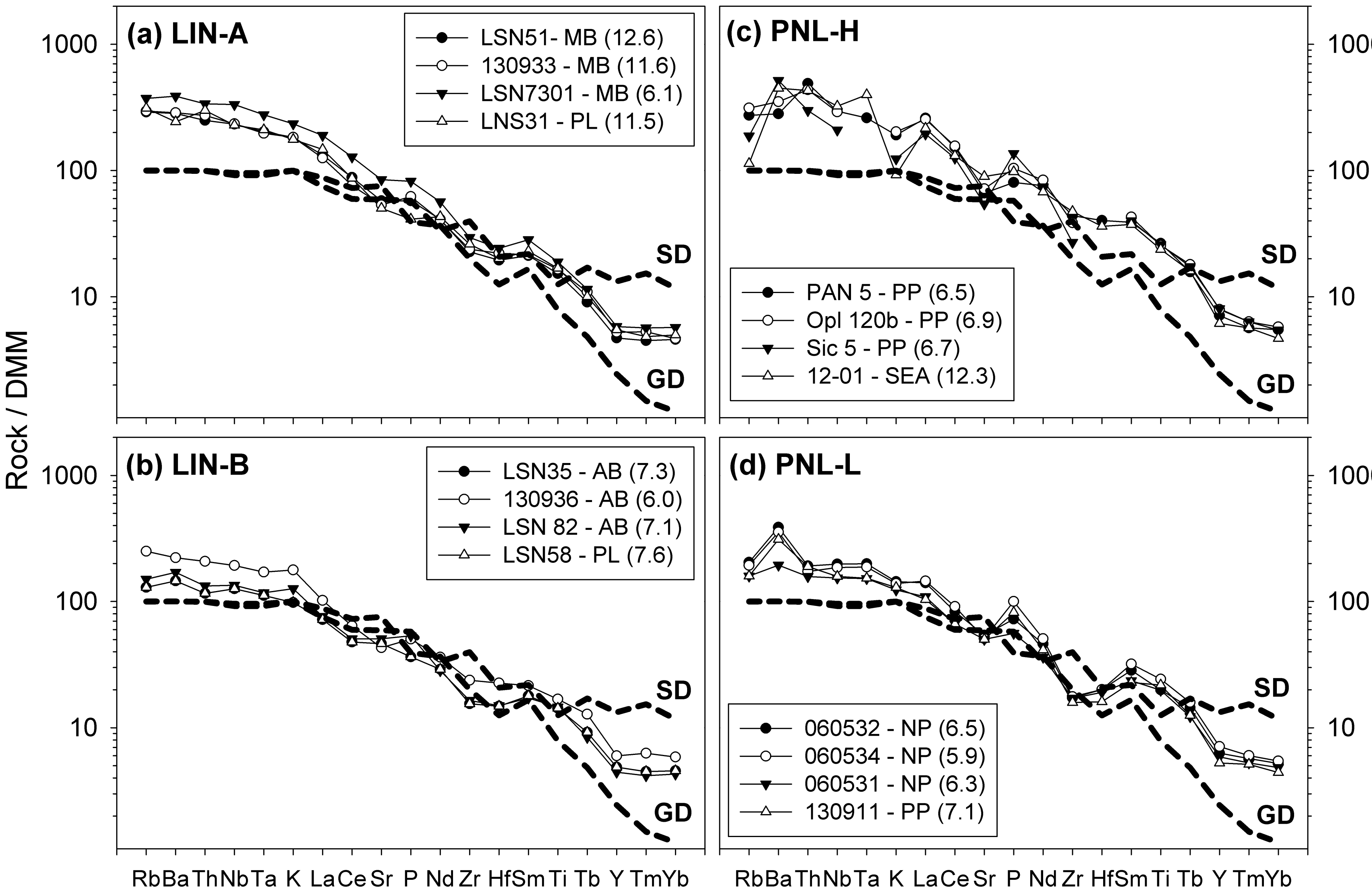

(a) LIN-A
LSN51- MB (12.6)
130933 - MB (11.6)
LSN7301 - MB (6.1)
LNS31 - PL (11.5)
(b) LIN-B
LSN35 - AB (7.3)
130936 - AB (6.0)
LSN 82 - AB (7.1)
LSN58 - PL (7.6)
(c) PNL-H
PAN 5 - PP (6.5)
Opl 120b - PP (6.9)
Sic 5 - PP (6.7)
12-01 - SEA (12.3)
(d) PNL-L
060532 - NP (6.5)
060534 - NP (5.9)
060531 - NP (6.3)
130911 - PP (7.1)
SD
GD
Rock / DMM
1000
100
10
Rb Ba Th Nb Ta K La Ce Sr P Nd Zr Hf Sm Ti Tb Y Tm Yb

Fig 7

Fig 8

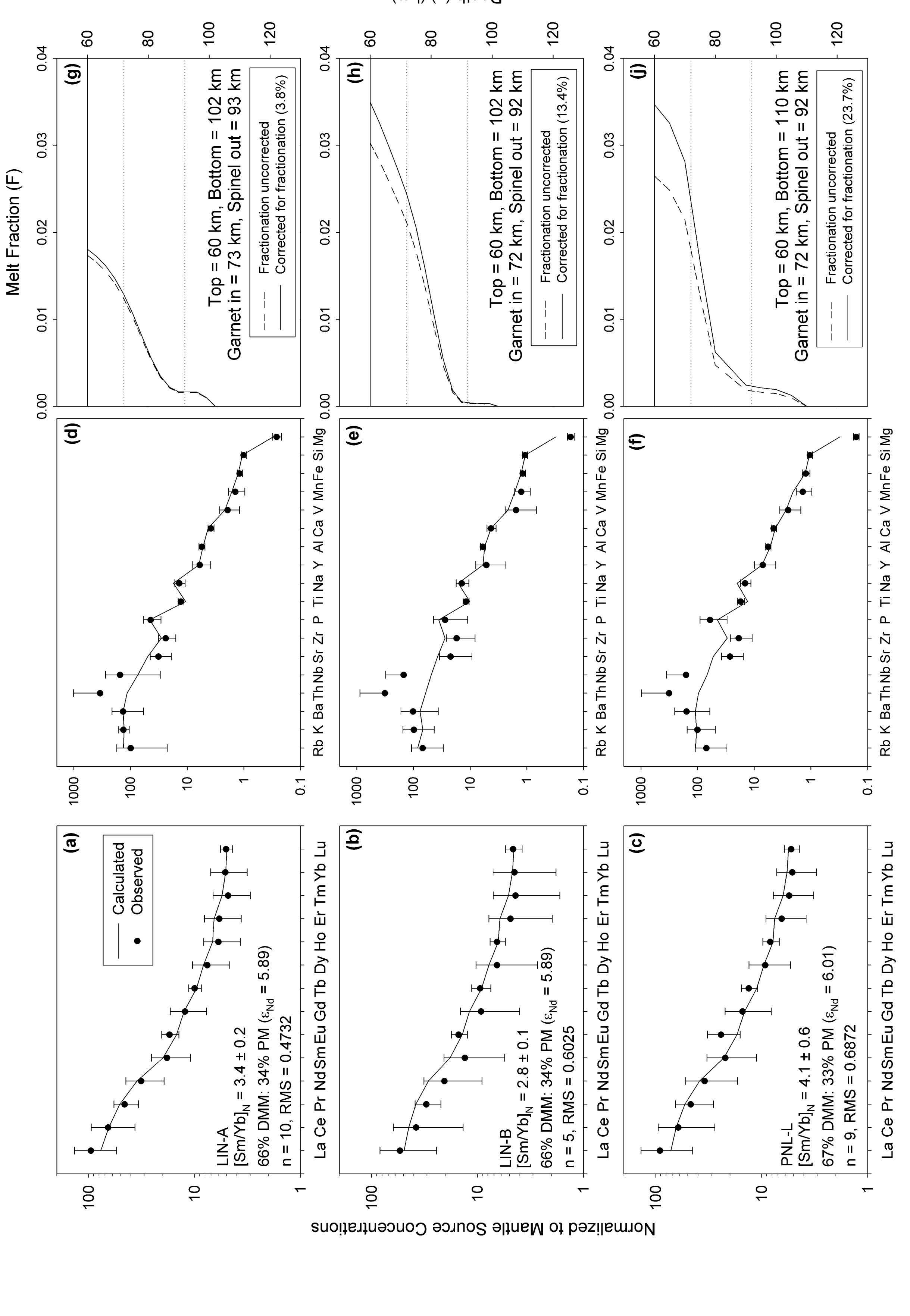

Normalized to Mantle Source Concentrations
Calculated
Observed
LIN-A
$[Sm/Yb]_N$ = 3.4 ± 0.2
66% DMM: 34% PM (ε_{Nd} = 5.89)
n = 10, RMS = 0.4732
LIN-B
$[Sm/Yb]_N$ = 2.8 ± 0.1
66% DMM: 34% PM (ε_{Nd} = 5.89)
n = 5, RMS = 0.6025
PNL-L
$[Sm/Yb]_N$ = 4.1 ± 0.6
67% DMM: 33% PM (ε_{Nd} = 6.01)
n = 9, RMS = 0.6872
La Ce Pr Nd Sm Eu Gd Tb Dy Ho Er Tm Yb Lu
Rb K Ba Th Nb Sr Zr P Ti Na Y Al Ca V Mn Fe Si Mg
Melt Fraction (F)
Depth (z) (km)
Top = 60 km, Bottom = 102 km
Garnet in = 73 km, Spinel out = 93 km
Fractionation uncorrected
Corrected for fractionation (3.8%)
Top = 60 km, Bottom = 102 km
Garnet in = 72 km, Spinel out = 92 km
Fractionation uncorrected
Corrected for fractionation (13.4%)
Top = 60 km, Bottom = 110 km
Garnet in = 72 km, Spinel out = 92 km
Fractionation uncorrected
Corrected for fractionation (23.7%)

Fig 9

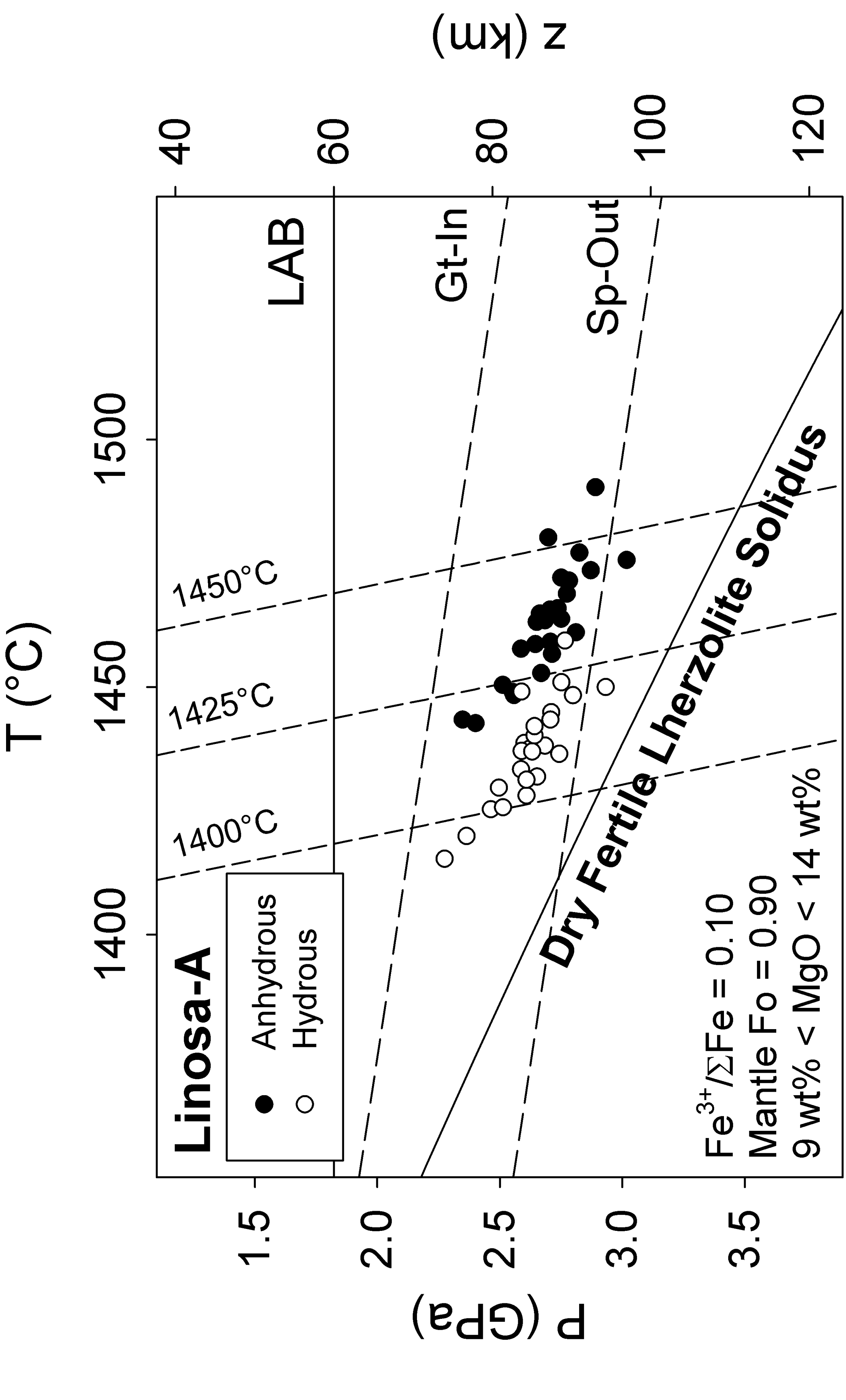

T (°C)
1400
1450
1500
z (km)
40
60
80
100
120
P (GPa)
1.5
2.0
2.5
3.0
3.5
LAB
Gt-In
Sp-Out
1400°C
1425°C
1450°C
Dry Fertile Lherzolite Solidus
Linosa-A
Anhydrous
Hydrous
Fe3+/ΣFe = 0.10
Mantle Fo = 0.90
9 wt% < MgO < 14 wt%

Fig 10

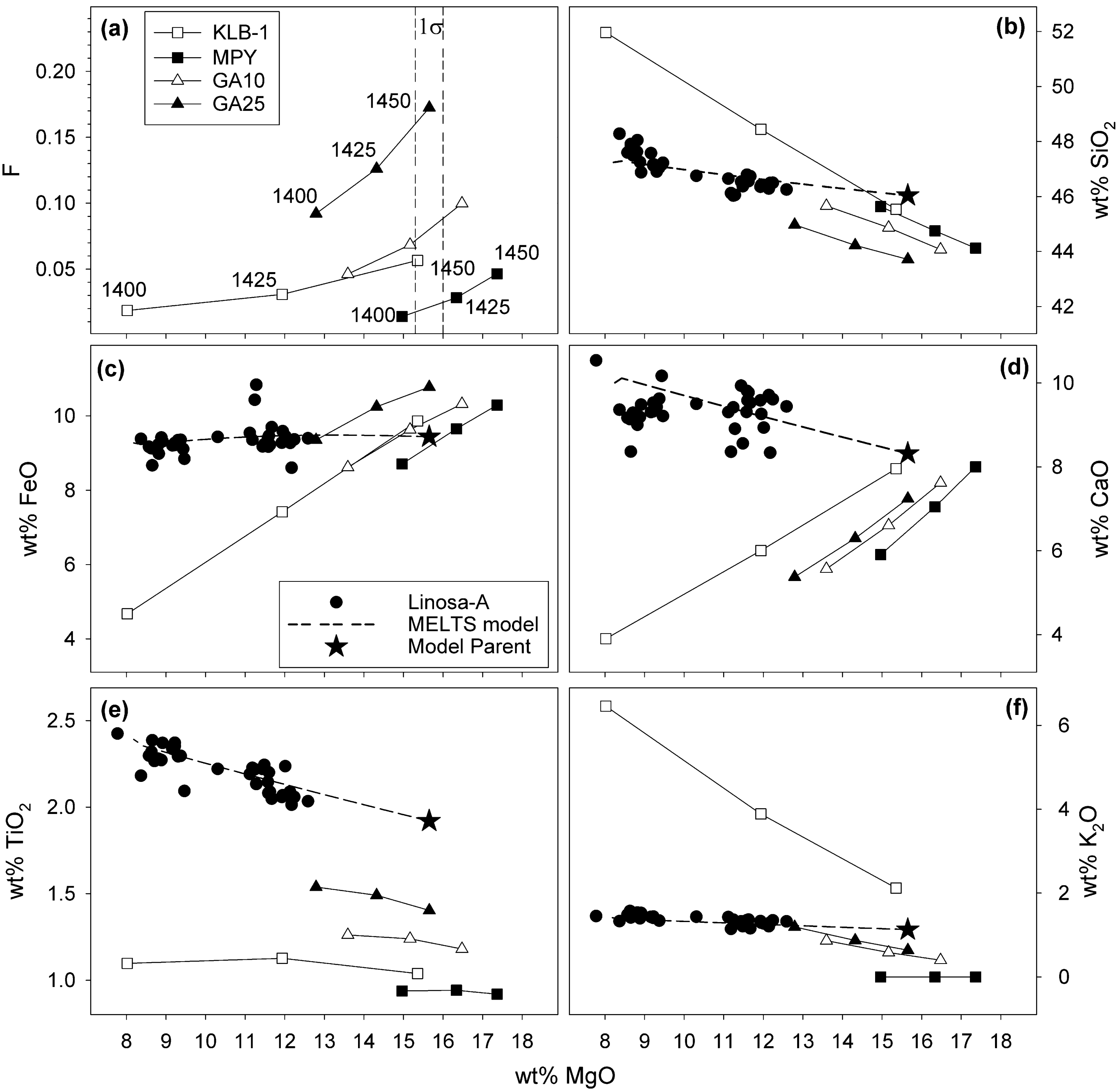

(a)
(b)
(c)
(d)
(e)
(f)
KLB-1
MPY
GA10
GA25
1σ
1400
1425
1450
F
wt% SiO_2
wt% FeO
wt% CaO
wt% TiO_2
wt% K_2O
wt% MgO
Linosa-A
MELTS model
Model Parent

Fig 11

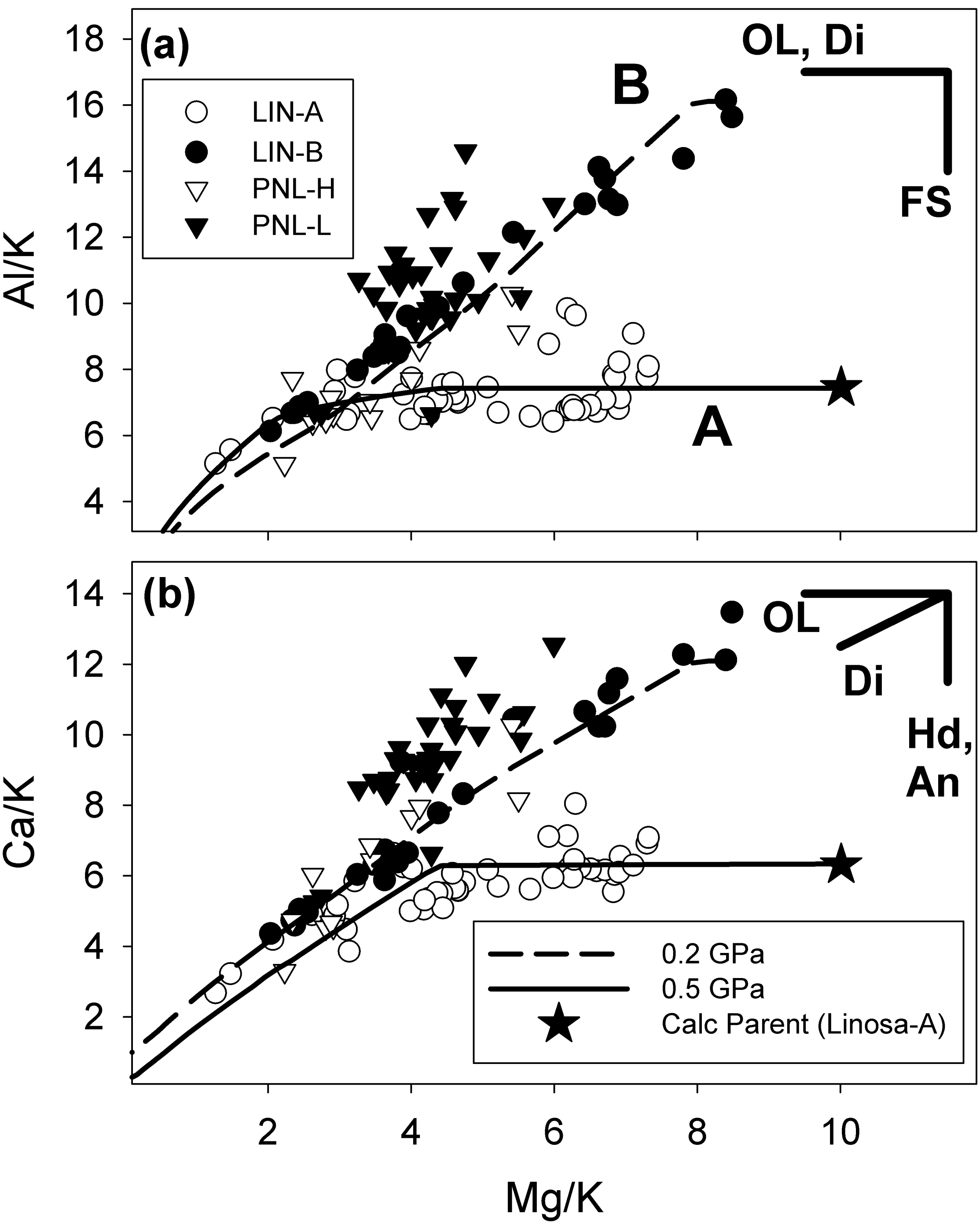
(a)
Al/K
18
16
14
12
10
8
6
4
LIN-A
LIN-B
PNL-H
PNL-L
B
OL, Di
FS
A
(b)
Ca/K
14
12
10
8
6
4
2
OL
Di
Hd,
An
0.2 GPa
0.5 GPa
Calc Parent (Linosa-A)
2
4
6
8
10
Mg/K

Table 1. Major and trace element compositions of volcanic rocks from Pantelleria and Linosa.

Island:	Pantelleria												Linosa										
Sample ID:	130912	130911	060532	030512	060531	030508	130916	060533	060534	130914	130913	130915	130934	130933	130931	130936	130937	130935	130939	130938	130941	130932
Phase:	PP	PP	NP	NP	NP	NP	PP	NP	NP	PP	PP	PP	MB	MB	MB	AB	AB	AB	MB	MB	AB	MB
Lat (N):	36.8353	36.8107	36.8311	36.8366	36.8269	36.8197	36.8261	36.8389	36.8361	36.8217	36.8214	36.8260	35.8745	35.8728	35.8643	36.8261	35.8629	35.8635	35.8624	35.8568	35.8580	35.8549
Long (E):	11.9691	11.9286	11.9367	11.9477	11.9556	11.9286	11.9364	11.9519	11.9678	11.9519	11.9287	11.9799	12.8709	12.8790	12.8815	11.9364	12.8545	12.8586	12.8620	12.8717	12.8676	12.8805
Class:	tB	aB	aB	tB	aB	AB	aB	aB	aB	aB	HAW	aB	aB	aB	aB	tB	HAW	HAW	tB	HAW	HAW	HAW
SiO_2, wt%	50.36	47.14	47.72	47.83	48.23	46.52	48.69	47.93	46.31	48.59	50.90	46.22	46.37	45.71	46.18	49.62	49.43	49.56	48.87	49.22	49.63	50.80
TiO_2	2.05	2.89	2.63	2.65	2.63	3.13	2.88	2.94	3.15	2.81	2.14	3.97	2.21	2.16	2.23	2.19	2.24	2.19	2.24	2.32	2.28	2.27
Al_2O_3	13.13	14.85	15.42	15.47	15.82	14.22	15.05	15.02	14.71	15.63	15.65	13.83	14.03	13.81	13.80	15.97	16.05	15.76	16.85	16.39	16.66	16.46
$Fe_2O_3^T$	10.50	13.22	11.72	12.14	11.94	13.63	12.98	12.66	12.89	12.79	10.62	15.58	11.68	11.87	12.03	11.50	11.46	11.36	11.04	11.26	11.19	11.14
MnO	0.17	0.19	0.17	0.16	0.16	0.18	0.19	0.18	0.18	0.18	0.18	0.22	0.18	0.18	0.18	0.17	0.17	0.17	0.14	0.18	0.18	0.18
MgO	7.43	7.08	6.44	6.27	6.23	6.12	5.87	5.82	5.79	5.78	5.66	5.15	11.40	11.39	11.28	5.93	5.84	5.63	5.20	5.10	5.10	4.79
CaO	9.69	10.65	11.17	11.08	11.33	10.48	10.69	10.56	10.57	10.89	9.42	10.27	9.90	9.41	9.45	8.98	8.95	8.83	10.50	8.91	8.74	8.66
Na_2O	2.98	3.28	3.21	2.92	3.09	3.16	3.35	3.52	3.33	3.27	3.61	3.41	3.20	2.97	3.23	3.73	3.87	3.86	3.22	4.04	4.22	4.39
K_2O	1.26	0.93	1.03	0.76	0.89	0.90	1.00	1.04	0.98	0.98	1.50	1.03	1.32	1.30	1.37	1.20	1.22	1.26	0.98	1.52	1.59	1.71
P_2O_5	0.64	0.76	0.67	0.48	0.52	0.61	0.65	0.72	0.91	0.64	0.46	1.35	0.52	0.57	0.58	0.48	0.47	0.46	0.40	0.62	0.62	0.61
LOI	0.24	-0.36	0.00	0.00	0.00	0.00	-0.67	0.00	0.00	-0.60	0.20	-0.88	0.11	-0.14	0.44	-0.34	0.03	-0.49	0.87	0.03	-0.46	-0.31
Total	98.45	100.63	100.19	99.77	100.84	98.95	100.68	100.40	98.82	100.96	100.34	100.15	100.92	99.23	100.77	99.44	99.73	98.59	100.32	99.59	99.75	100.70
Mg#	0.61	0.54	0.55	0.53	0.53	0.50	0.50	0.50	0.50	0.50	0.54	0.42	0.68	0.68	0.67	0.53	0.53	0.52	0.51	0.50	0.50	0.49
Sc, ppm	22	31	30	32	31	33	32	30	30	31	25	30	26	26	24	23	22	22	29	23	22	22
V	176	307	274	280	295	323	320	312	320	313	226	374	233	228	219	206	202	204	236	204	199	205
Cr	270	90	130	101	120	91	100	100	70	100	100	30	450	490	420	180	160	160	290	120	100	100
Co	37	43	36	64	39	58	38	29	35	38	32	38	50	53	51	35	34	33	32	31	28	29
Ni	170	80	65	57	60	57	50	41	43	150	70	40	250	270	250	80	80	70	70	60	60	50
Cu	20	40	53	n.a.	78	n.a.	40	33	44	40	50	20	50	60	50	60	60	40	60	30	40	40
Zn	130	90	75	94	76	103	100	80	82	100	110	180	80	90	90	110	100	100	170	100	100	110
Ga	22	19	19	17	20	17	21	16	19	21	22	22	18	18	18	21	21	21	20	22	22	23
Ge	1.8	1.7	1.1	1.6	1.1	1.6	2	0.9	1.2	1.6	1.7	1.7	1.6	1.5	1.7	1.6	1.8	1.7	2.3	1.7	1.6	1.7
Rb	39	14	18	12	14	13	16	13	17	15	25	15	25	26	26	22	22	22	16	27	29	30
Sr	523	492	530	485	492	421	472	491	499	481	418	515	537	523	606	411	427	422	446	467	488	460
Y	45.0	21.4	25.6	22.1	23.9	25.3	24.4	22.2	28.9	23.9	32	31.2	20.1	21.3	22.1	24.5	24.1	24.4	22	28.9	28.9	30.3
Zr	454	126	137	128	136	139	147	153	140	145	239	158	194	189	200	186	187	189	139	237	239	259
Nb	106.0	33.2	41.6	53.5	32.3	36.1	39.4	36.2	39.1	37.6	59.8	42.2	46.4	49.2	49.6	40.6	41.3	40.5	28.3	52	52.4	56.2
Ba	288	373	465	219	233	304	335	348	426	338	409	378	342	344	344	257	261	267	184	321	330	344
La	71.80	24.3	32.9	26.0	25.5	28.80	25.6	28.9	34	25.2	38.3	34.1	29.6	29.4	32	24.5	22.7	23.9	16.5	31.2	30.4	33.5
Ce	136.00	51.3	64.3	49.6	51.3	56.77	54.5	59.6	70.4	53.1	72.6	73.5	60.1	58.9	64.1	51.1	46.8	49.5	35.5	63	62.9	67.4
Pr	15.80	6.67	8.24	6.12	6.56	6.98	6.97	7.37	9.15	6.74	9.24	9.98	7.17	7.29	7.69	6.24	5.91	6.17	4.59	7.77	7.55	8.28
Nd	59.20	29.5	32.9	27.4	25.8	31.04	30.4	28.4	36.2	29.6	37	44	28.9	28.9	30.7	25.6	24.4	25.8	19.8	31.8	32.1	33.7
Sm	11.90	6.17	7.7	6.35	6.37	7.37	6.76	6.92	8.64	6.63	7.45	9.4	5.71	5.79	6.33	5.78	5.49	5.82	4.96	7.07	6.94	7.02
Eu	2.75	2.65	3.02	2.30	2.37	2.74	2.65	2.59	3.58	2.44	2.53	3.66	2	1.92	2.1	1.93	1.9	2.01	1.74	2.34	2.29	2.31
Gd	10.80	6.54	6.87	6.39	5.89	7.32	6.59	5.95	7.93	6.35	7.5	9.66	5.65	5.56	5.98	5.83	5.76	6.04	5.02	6.75	6.75	6.9
Tb	1.72	0.94	1.08	1.02	0.92	1.12	1.01	0.97	1.19	0.96	1.18	1.41	0.84	0.82	0.87	0.96	0.88	0.96	0.79	1.05	1.04	1.1
Dy	9.46	5.17	5.61	5.24	5.07	5.91	5.38	5.4	6.1	5.16	6.59	7.22	4.57	4.49	4.67	5.06	5.01	5.19	4.51	5.99	5.77	6.39
Ho	1.75	0.92	0.94	0.95	0.87	1.07	0.95	0.94	1.05	0.95	1.24	1.28	0.84	0.79	0.89	0.94	0.92	0.95	0.82	1.12	1.09	1.18
Er	4.96	2.38	2.5	2.54	2.28	2.82	2.52	2.5	2.79	2.54	3.24	3.21	2.29	2.18	2.4	2.63	2.52	2.61	2.32	3.14	3.11	3.43
Tm	0.73	0.308	0.342	0.332	0.316	0.38	0.323	0.346	0.361	0.317	0.482	0.438	0.34	0.317	0.339	0.394	0.369	0.377	0.323	0.461	0.432	0.494
Yb	4.49	1.80	2.12	1.94	1.97	2.19	1.9	2.11	2.22	2	2.9	2.52	1.99	1.87	2.14	2.33	2.3	2.35	1.91	2.8	2.89	3.04
Lu	0.64	0.262	0.3	0.296	0.288	0.33	0.298	0.294	0.319	0.294	0.393	0.345	0.295	0.276	0.3	0.312	0.326	0.316	0.272	0.422	0.422	0.439
Hf	10.80	3.2	4	4.2	3.8	4.29	3.7	4	4	3.5	5.5	3.9	4.6	4.4	4.5	4.4	4.3	4.5	3.2	5.2	5.1	5.6
Ta	5.96	2.11	2.75	2.97	2.1	3.17	2.18	2.51	2.59	2.28	3.43	2.64	2.73	2.72	3.29	2.55	2.28	2.36	1.73	3.03	2.89	3.27
Th	10.10	2.59	2.62	2.10	2.16	2.20	2.58	2.38	2.37	2.72	4.71	3.01	3.99	3.74	4.06	2.88	2.74	2.85	1.74	4.27	4.12	4.16
U	2.88	0.55	3.13	0.67	2.26	0.63	0.72	2.37	1.8	0.64	1.36	0.53	1.51	1.14	1.25	0.82	0.87	0.88	0.56	1.09	1.16	1.2

Phases of mafic volcanism for Pantelleria (following Civetta et al., 1998; Avanzinelli et al., 2004); PP, paleo-Pantelleria (120 and 80 ka); NP, neo-Pantelleria (29 and 10 ka). Phases of mafic volcanism for Linosa (following Lanzafame et al., 1994): AB, Arena Bianca (700 ka); MB, Monte Bandiera (530 ka).
Class (Le Maitre, 2002): aB, Alkali Basalt; tB, Transitional Basalt; HAW, Hawaiite. $Fe_2O_3^T$, total iron reported as Fe_2O_3; LOI, Loss on Ignition; Mg# = mol Mg/(Mg+Fe^{2+}), assuming Fe^{2+} = 0.9Fe^T; n.a., not analyzed.

Table 2. Summary of the results of pMELTS models of isentropic partial melting (3.0 - 1.8 GPa) under anhydrous conditions and $f O_2$ = FMQ(T,P)

		Mantle Source			Calculated Melt Parameters			Original Misfit (wt%)		Adjusted Primary Basalt / Misfit (wt%)							
Material	T_P (°C)	Mantle	%Lherz	%MORB	LAB T (°C)	wt% TiO_2	Mg#	CMAS	+TNK	Mg#	$T^{ol\text{-}liq}$ (°C)	$P^{ol\text{-}liq}$ (GPa)	Fo_{mantle}	%F	wt% TiO_2	CMAS	+TNK
KLB1	1450	PM	100	0	1434	1.04	76.1	4.11	6.88	73.45	1455	2.59	0.90	3.3	1.94	3.84	6.59
MPY	1450	DM	100	0	1429	0.92	77.6	6.16	10.75	75.70	1513	3.18	0.91	-4.5	1.82	4.70	9.26
MPY+GA1	1450	DM	90	10	1420	1.18	76.6	6.07	10.16	74.77	1488	2.92	0.90	-1.1	1.87	5.21	9.30
MPY+GA1	1450	DM	75	25	1411	1.40	74.9	5.90	9.73	73.85	1464	2.69	0.90	2.1	1.92	5.89	9.72
MPY	1425	DM	100	0	1413	0.94	77.7	6.59	12.57	74.62	1484	2.88	0.90	-4.4	1.88	5.94	11.90
MPY+GA1	1450	DM	62.5	37.5	1405	1.50	73.3	6.78	10.50	73.03	1445	2.51	0.90	4.7	1.96	6.13	9.88
MPY+GA1	1450	DM	50	50	1398	1.61	71.3	7.99	11.70	71.51	1412	2.22	0.89	9.2	2.02	6.23	9.97
MPY+GA1	1425	DM	90	10	1403	1.24	76.5	7.25	12.53	73.20	1449	2.54	0.90	0.3	1.95	6.79	12.06
MPY+GA1	1425	DM	50	50	1381	1.72	70.1	10.39	14.88	69.82	1378	1.96	0.88	10.1	2.09	7.31	11.84
MPY+GA1	1425	DM	75	25	1393	1.49	74.3	8.86	13.66	72.16	1425	2.33	0.89	3.6	2.00	7.34	12.18
MPY+GA1	1425	DM	62.5	37.5	1387	1.60	72.3	9.69	14.32	71.23	1408	2.19	0.89	5.9	2.03	7.55	12.21
MPY	1400	DM	100	0	1393	0.94	78.2	8.36	16.22	72.95	1443	2.49	0.90	-2.7	1.96	7.67	15.20
MPY+GA1	1400	DM	90	10	1384	1.26	76.8	10.68	17.27	71.13	1404	2.16	0.89	2.7	2.04	8.45	15.08
MPY+GA1	1400	DM	50	50	1362	1.80	69.2	13.39	19.16	67.75	1340	1.69	0.87	11.5	2.18	8.66	14.23
MPY+GA1	1400	DM	75	25	1374	1.54	74.1	12.04	18.06	70.03	1382	1.99	0.88	5.7	2.09	8.87	14.83
MPY+GA1	1400	DM	62.5	37.5	1368	1.67	71.7	12.74	18.74	69.06	1366	1.87	0.88	7.9	2.12	9.00	14.85
MPY+GA1	1450	DM	25	75	1372	2.11	65.3	19.06	22.80	62.54	1270	1.27	0.85	29.0	2.34	9.73	13.20
KLB1	1425	PM	100	0	1415	1.13	77.0	14.95	20.92	68.49	1358	1.81	0.88	12.8	2.14	9.90	15.76
KG2	1450	PM	67	33	1404	1.44	70.2	11.06	14.12	74.24	1474	2.78	0.90	0.8	1.90	10.69	13.74
KG1	1450	PM	50	50	1401	1.62	68.2	11.24	14.37	73.85	1464	2.69	0.90	2.1	1.92	11.18	14.31
KG2	1400	PM	67	33	1369	1.68	68.4	13.58	18.43	70.54	1394	2.08	0.89	4.0	2.06	11.18	16.07
KG2	1425	PM	67	33	1387	1.59	69.0	12.20	16.13	72.60	1435	2.42	0.89	2.2	1.98	11.30	15.25
MPY+GA1	1425	DM	25	75	1356	2.32	64.1	22.45	27.00	60.04	1242	1.13	0.84	29.2	2.40	11.67	15.55
KG1	1425	PM	50	50	1382	1.79	66.5	13.53	17.52	72.07	1423	2.32	0.89	3.9	2.00	12.24	16.25
KG1	1400	PM	50	50	1363	1.91	65.4	15.17	20.09	70.03	1382	1.99	0.88	5.7	2.09	12.35	17.31
MPY+GA1	1400	DM	25	75	1339	2.50	63.3	26.09	31.87	57.14	1214	1.00	0.82	29.4	2.47	14.66	19.00
KLB1	1400	PM	100	0	1395	1.10	78.5	28.50	38.32	60.63	1248	1.16	0.84	24.5	2.38	18.20	27.58

Material: See text for details; T_P: Mantle potential temperature; Mantle: PM, Primitive Mantle; DM, Depleted Mantle; PXN, Pyroxenite; %Lherz-%MORB: Relative abundances of each component in peridotite:pyroxenite mixtures; LAB T: final (lithosphere-asthenosphere) melt temperature; Mg# = 100*Mg/(Mg+Fe^{2+}); CMAS: sum of the absolute differences between the pMELTS result and the calculated primary melt of CaO + MgO + FeO + Fe_2O_3 + Al_2O_3 + SiO_2; +TNK: Same as CMAS, plus TiO_2+Na_2O+K_2O. Original misfit results compare the final pMELTS liquid with the one calculated from Lee et al. (2009); Adjusted primary basalt paramters are for the misfit-minimized melt composition following Schorttle and Maclennan (2011) (see text for details.) $T^{ol\text{-}liq}$ and $P^{ol\text{-}liq}$ are the recalculated average temperatures and pressures of melt segregation calculated following Lee et al. (2009); Fo_{mantle} is the composition of olivine in the mantle in equilibrium with the recalculated primary basalt; %F is an estimate of the degree of partial melting following Putrika et al. (2007): %F = $100(T_0(P^{ol\text{-}liq}) - T^{ol\text{-}liq})C_P/\Delta H_{fus}$ and $T_0(P^{ol\text{-}liq}) = T_P \exp(10000 P \alpha V/C_P)$, where C_P = 192.4 J mol^{-1} K^{-1}, ΔH_{fus} = 128.3 kJ mol^{-1}, $\alpha = 3 \times 10^{-5}$ K^{-1}. Pressure (P) is in GPa. Negative values of %F suggest that the calculated olivine-liquid temperature of the recalculated basalt exceed the experimental mantle conditions given the constants chosen.